Draft version April 25, 2014
Preprint typeset using LaTeX style emulateapj v. 12/16/11

GRAVITATIONAL WAVES FROM KNOWN PULSARS: RESULTS FROM THE INITIAL DETECTOR ERA

J. Aasi[1], J. Abadie[1], B. P. Abbott[1], R. Abbott[1], T. Abbott[2], M. R. Abernathy[1], T. Accadia[3], F. Acernese[4,5], C. Adams[6], T. Adams[7], R. X. Adhikari[1], C. Affeldt[8], M. Agathos[9], N. Aggarwal[10], O. D. Aguiar[11], P. Ajith[1], B. Allen[8,12,13], A. Allocca[14,15], E. Amador Ceron[12], D. Amariutei[16], R. A. Anderson[1], S. B. Anderson[1], W. G. Anderson[12], K. Arai[1], M. C. Araya[1], C. Arceneaux[17], J. Areeda[18], S. Ast[13], S. M. Aston[6], P. Astone[19], P. Aufmuth[13], C. Aulbert[8], L. Austin[1], B. E. Aylott[20], S. Babak[21], P. T. Baker[22], G. Ballardin[23], S. W. Ballmer[24], J. C. Barayoga[1], D. Barker[25], S. H. Barnum[10], F. Barone[4,5], B. Barr[26], L. Barsotti[10], M. Barsuglia[27], M. A. Barton[25], I. Bartos[28], R. Bassiri[29,26], A. Basti[14,30], J. Batch[25], J. Bauchrowitz[8], Th. S. Bauer[9], M. Bebronne[3], B. Behnke[21], M. Bejger[31], M. G. Beker[9], A. S. Bell[26], C. Bell[26], I. Belopolski[28], G. Bergmann[8], J. M. Berliner[25], D. Bersanetti[32,33], A. Bertolini[9], D. Bessis[34], J. Betzwieser[6], P. T. Beyersdorf[35], T. Bhadbhade[29], I. A. Bilenko[36], G. Billingsley[1], J. Birch[6], M. Bitossi[14], M. A. Bizouard[37], E. Black[1], J. K. Blackburn[1], L. Blackburn[38], D. Blair[39], M. Blom[9], O. Bock[8], T. P. Bodiya[10], M. Boer[40], C. Bogan[8], C. Bond[20], F. Bondu[41], L. Bonelli[14,30], R. Bonnand[42], R. Bork[1], M. Born[8], V. Boschi[14], S. Bose[43], L. Bosi[44], J. Bowers[2], C. Bradaschia[14], P. R. Brady[12], V. B. Braginsky[36], M. Branchesi[45,46], C. A. Brannen[43], J. E. Brau[47], J. Breyer[8], T. Briant[48], D. O. Bridges[6], A. Brillet[40], M. Brinkmann[8], V. Brisson[37], M. Britzger[8], A. F. Brooks[1], D. A. Brown[24], D. D. Brown[20], F. Brückner[20], T. Bulik[49], H. J. Bulten[9,50], A. Buonanno[51], D. Buskulic[3], C. Buy[27], R. L. Byer[29], L. Cadonati[52], G. Cagnoli[42], J. Calderón Bustillo[53], E. Calloni[4,54], J. B. Camp[38], P. Campsie[26], K. C. Cannon[55], B. Canuel[23], J. Cao[56], C. D. Capano[51], F. Carbognani[23], L. Carbone[20], S. Caride[57], A. Castiglia[58], S. Caudill[12], M. Cavaglià[17], F. Cavalier[37], R. Cavalieri[23], G. Cella[14], C. Cepeda[1], E. Cesarini[59], R. Chakraborty[1], T. Chalermsongsak[1], S. Chao[60], P. Charlton[61], E. Chassande-Mottin[27], X. Chen[39], Y. Chen[62], A. Chincarini[32], A. Chiummo[23], H. S. Cho[63], J. Chow[64], N. Christensen[65], Q. Chu[39], S. S. Y. Chua[64], S. Chung[39], G. Ciani[16], F. Clara[25], D. E. Clark[29], J. A. Clark[52], F. Cleva[40], E. Coccia[66,67], P.-F. Cohadon[48], A. Colla[19,68], M. Colombini[44], M. Constancio Jr.[11], A. Conte[19,68], R. Conte[69], D. Cook[25], T. R. Corbitt[2], M. Cordier[35], N. Cornish[22], A. Corsi[70], C. A. Costa[11], M. W. Coughlin[71], J.-P. Coulon[40], S. Countryman[28], P. Couvares[24], D. M. Coward[39], M. Cowart[6], D. C. Coyne[1], K. Craig[26], J. D. E. Creighton[12], T. D. Creighton[34], S. G. Crowder[72], A. Cumming[26], L. Cunningham[26], E. Cuoco[23], K. Dahl[8], T. Dal Canton[8], M. Damjanic[8], S. L. Danilishin[39], S. D'Antonio[59], K. Danzmann[8,13], V. Dattilo[23], B. Daudert[1], H. Daveloza[34], M. Davier[37], G. S. Davies[26], E. J. Daw[73], R. Day[23], T. Dayanga[43], R. De Rosa[4,54], G. Debreczeni[74], J. Degallaix[42], W. Del Pozzo[9], E. Deleeuw[16], S. Deléglise[48], T. Denker[8], T. Dent[8], H. Dereli[40], V. Dergachev[1], R. DeRosa[2], R. DeSalvo[69], S. Dhurandhar[75], L. Di Fiore[4], A. Di Lieto[14,30], I. Di Palma[8], A. Di Virgilio[14], M. Díaz[34], A. Dietz[17], K. Dmitry[36], F. Donovan[10], K. L. Dooley[8], S. Doravari[6], M. Drago[76,77], R. W. P. Drever[78], J. C. Driggers[1], Z. Du[56], J. -C. Dumas[39], S. Dwyer[25], T. Eberle[8], M. Edwards[7], A. Effler[2], P. Ehrens[1], J. Eichholz[16], S. S. Eikenberry[16], G. Endrőczi[74], R. Essick[10], T. Etzel[1], K. Evans[26], M. Evans[10], T. Evans[6], M. Factourovich[28], V. Fafone[59,67], S. Fairhurst[7], Q. Fang[39], S. Farinon[32], B. Farr[79], W. Farr[79], M. Favata[80], D. Fazi[79], H. Fehrmann[8], D. Feldbaum[16,6], I. Ferrante[14,30], F. Ferrini[23], F. Fidecaro[14,30], L. S. Finn[81], I. Fiori[23], R. Fisher[24], R. Flaminio[42], E. Foley[18], S. Foley[10], E. Forsi[6], N. Fotopoulos[1], J.-D. Fournier[40], S. Franco[37], S. Frasca[19,68], F. Frasconi[14], M. Frede[8], M. Frei[58], Z. Frei[82], A. Freise[20], R. Frey[47], T. T. Fricke[8], P. Fritschel[10], V. V. Frolov[6], M.-K. Fujimoto[83], P. Fulda[16], M. Fyffe[6], J. Gair[71], L. Gammaitoni[44,84], J. Garcia[25], F. Garufi[4,54], N. Gehrels[38], G. Gemme[32], E. Genin[23], A. Gennai[14], L. Gergely[82], S. Ghosh[43], J. A. Giaime[2,6], S. Giampanis[12], K. D. Giardina[6], A. Giazotto[14], S. Gil-Casanova[53], C. Gill[26], J. Gleason[16], E. Goetz[8], R. Goetz[16], L. Gondan[82], G. González[2], N. Gordon[26], M. L. Gorodetsky[36], S. Gossan[62], S. Gossler[8], R. Gouaty[3], C. Graef[8], P. B. Graff[38], M. Granata[42], A. Grant[26], S. Gras[10], C. Gray[25], R. J. S. Greenhalgh[85], A. M. Gretarsson[86], C. Griffo[18], P. Groot[87], H. Grote[8], K. Grover[20], S. Grunewald[21], G. M. Guidi[45,46], C. Guido[6], K. E. Gushwa[1], E. K. Gustafson[1], R. Gustafson[57], B. Hall[43], E. Hall[1], D. Hammer[12], G. Hammond[26], M. Hanke[8], J. Hanks[25], C. Hanna[88], J. Hanson[6], J. Harms[1], G. M. Harry[89], I. W. Harry[24], E. D. Harstad[47], M. T. Hartman[16], K. Haughian[26], K. Hayama[83], J. Heefner[†,1], A. Heidmann[48], M. Heintze[16,6], H. Heitmann[40], P. Hello[37], G. Hemming[23], M. Hendry[26], I. S. Heng[26], A. W. Heptonstall[1], M. Heurs[8], S. Hild[26], D. Hoak[52], K. A. Hodge[1], K. Holt[6], M. Holtrop[90], T. Hong[62], S. Hooper[39], T. Horrom[91], D. J. Hosken[92], J. Hough[26], E. J. Howell[39], Y. Hu[26], Z. Hua[56], V. Huang[60], E. A. Huerta[24], B. Hughey[86], S. Husa[53], S. H. Huttner[26], M. Huynh[12], T. Huynh-Dinh[6], J. Iafrate[2], D. R. Ingram[25], R. Inta[64], T. Isogai[10], A. Ivanov[1], B. R. Iyer[93], K. Izumi[25], M. Jacobson[1], E. James[1], H. Jang[94], Y. J. Jang[79], P. Jaranowski[95], F. Jiménez-Forteza[53], W. W. Johnson[2], D. Jones[25], D. I. Jones[96], R. Jones[26], R. J. G. Jonker[9], L. Ju[39], Haris K[97], P. Kalmus[1], V. Kalogera[79], S. Kandhasamy[72], G. Kang[94], J. B. Kanner[38], M. Kasprzack[23,37], R. Kasturi[98], E. Katsavounidis[10], W. Katzman[6], H. Kaufer[13], K. Kaufman[62], K. Kawabe[25], S. Kawamura[83], F. Kawazoe[8], F. Kéfélian[40], D. Keitel[8], D. B. Kelley[24], W. Kells[1], D. G. Keppel[8], A. Khalaidovski[8], F. Y. Khalili[36], E. A. Khazanov[99], B. K. Kim[94], C. Kim[100,94], K. Kim[101], N. Kim[29], W. Kim[92], Y.-M. Kim[63], E. J. King[92], P. J. King[1], D. L. Kinzel[6], J. S. Kissel[10], S. Klimenko[16], J. Kline[12], S. Koehlenbeck[8], K. Kokeyama[2], V. Kondrashov[1], S. Koranda[12], W. Z. Korth[1], I. Kowalska[49], D. Kozak[1], A. Kremin[72], V. Kringel[8], B. Krishnan[8], A. Królak[102,103], C. Kucharczyk[29], S. Kudla[2], G. Kuehn[8], A. Kumar[104], P. Kumar[24], R. Kumar[26], R. Kurdyumov[29], P. Kwee[10], M. Landry[25], B. Lantz[29], S. Larson[105], P. D. Lasky[106], C. Lawrie[26], A. Lazzarini[1], A. Le Roux[6], P. Leaci[21], E. O. Lebigot[56], C.-H. Lee[63], H. K. Lee[101], H. M. Lee[100], J. Lee[10], J. Lee[18], M. Leonardi[76,77], J. R. Leong[8], N. Leroy[37], N. Letendre[3], B. Levine[25], J. B. Lewis[1], V. Lhuillier[25], T. G. F. Li[9], A. C. Lin[29], T. B. Littenberg[79], V. Litvine[1], F. Liu[107], H. Liu[7], Y. Liu[56], Z. Liu[16], D. Lloyd[1], N. A. Lockerbie[108], V. Lockett[18], D. Lodhia[20], K. Loew[86], J. Logue[26], A. L. Lombardi[52], M. Lorenzini[59], V. Loriette[109], M. Lormand[6], G. Losurdo[45], J. Lough[24], J. Luan[62], M. J. Lubinski[25], H. Lück[8,13], A. P. Lundgren[8], J. Macarthur[26], E. Macdonald[7], B. Machenschalk[8],

M. MacInnis[10], D. M. Macleod[7], F. Magana-Sandoval[18], M. Mageswaran[1], K. Mailand[1], E. Majorana[19], I. Maksimovic[109], V. Malvezzi[59], N. Man[40], G. M. Manca[8], I. Mandel[20], V. Mandic[72], V. Mangano[19,68], M. Mantovani[14], F. Marchesoni[44,110], F. Marion[3], S. Márka[28], Z. Márka[28], A. Markosyan[29], E. Maros[1], J. Marque[23], F. Martelli[45,46], I. W. Martin[26], R. M. Martin[16], L. Martinelli[40], D. Martynov[1], J. N. Marx[1], K. Mason[10], A. Masserot[3], T. J. Massinger[24], F. Matichard[10], L. Matone[28], R. A. Matzner[111], N. Mavalvala[10], G. May[2], N. Mazumder[97], G. Mazzolo[8], R. McCarthy[25], D. E. McClelland[64], S. C. McGuire[112], G. McIntyre[1], J. McIver[52], D. Meacher[40], G. D. Meadors[57], M. Mehmet[8], J. Meidam[9], T. Meier[13], A. Melatos[106], G. Mendell[25], R. A. Mercer[12], S. Meshkov[1], C. Messenger[26], M. S. Meyer[6], H. Miao[62], C. Michel[42], E. E. Mikhailov[91], L. Milano[4,54], J. Miller[64], Y. Minenkov[59], C. M. F. Mingarelli[20], S. Mitra[75], V. P. Mitrofanov[36], G. Mitselmakher[16], R. Mittleman[10], B. Moe[12], M. Mohan[23], S. R. P. Mohapatra[24,58], F. Mokler[8], D. Moraru[25], G. Moreno[25], N. Morgado[42], T. Mori[83], S. R. Morriss[34], K. Mossavi[8], B. Mours[3], C. M. Mow-Lowry[8], C. L. Mueller[16], G. Mueller[16], S. Mukherjee[34], A. Mullavey[2], J. Munch[92], D. Murphy[28], P. G. Murray[26], A. Mytidis[16], M. F. Nagy[74], D. Nanda Kumar[16], I. Nardecchia[19,68], T. Nash[1], L. Naticchioni[19,68], R. Nayak[113], V. Necula[16], G. Nelemans[87,9], I. Neri[44,84], M. Neri[32,33], G. Newton[26], T. Nguyen[64], E. Nishida[83], A. Nishizawa[83], A. Nitz[24], F. Nocera[23], D. Nolting[6], M. E. Normandin[34], L. K. Nuttall[7], E. Ochsner[12], J. O'Dell[85], E. Oelker[10], G. H. Ogin[1], J. J. Oh[114], S. H. Oh[114], F. Ohme[7], P. Oppermann[8], B. O'Reilly[6], W. Ortega Larcher[34], R. O'Shaughnessy[12], C. Osthelder[1], D. J. Ottaway[92], R. S. Ottens[16], J. Ou[60], H. Overmier[6], B. J. Owen[81], C. Padilla[18], A. Pai[97], C. Palomba[19], Y. Pan[51], C. Pankow[12], F. Paoletti[14,23], R. Paoletti[14,15], M. A. Papa[21,12], H. Paris[25], A. Pasqualetti[23], R. Passaquieti[14,30], D. Passuello[14], M. Pedraza[1], P. Peiris[58], S. Penn[98], A. Perreca[24], M. Phelps[1], M. Pichot[40], M. Pickenpack[8], F. Piergiovanni[45,46], V. Pierro[69], L. Pinard[42], B. Pindor[106], I. M. Pinto[69], M. Pitkin[26], J. Poeld[8], R. Poggiani[14,30], V. Poole[43], C. Poux[1], V. Predoi[7], T. Prestegard[72], L. R. Price[1], M. Prijatelj[8], M. Principe[69], S. Privitera[1], R. Prix[8], G. A. Prodi[76,77], L. Prokhorov[36], O. Puncken[34], M. Punturo[44], P. Puppo[19], V. Quetschke[34], E. Quintero[1], R. Quitzow-James[47], F. J. Raab[25], D. S. Rabeling[9,50], I. Rácz[74], H. Radkins[25], P. Raffai[28,82], S. Raja[115], G. Rajalakshmi[116], M. Rakhmanov[34], C. Ramet[6], P. Rapagnani[19,68], V. Raymond[1], V. Re[59,67], C. M. Reed[25], T. Reed[117], T. Regimbau[40], S. Reid[118], D. H. Reitze[1,16], F. Ricci[19,68], R. Riesen[6], K. Riles[57], N. A. Robertson[1,26], F. Robinet[37], A. Rocchi[59], S. Roddy[6], C. Rodriguez[79], M. Rodruck[25], C. Roever[8], L. Rolland[3], J. G. Rollins[1], J. D. Romano[34], R. Romano[4,5], G. Romanov[91], J. H. Romie[6], D. Rosińska[31,119], S. Rowan[26], A. Rüdiger[8], P. Ruggi[23], K. Ryan[25], F. Salemi[8], L. Sammut[106], V. Sandberg[25], J. Sanders[57], V. Sannibale[1], I. Santiago-Prieto[26], E. Saracco[42], B. Sassolas[42], B. S. Sathyaprakash[7], P. R. Saulson[24], R. Savage[25], R. Schilling[8], R. Schnabel[8,13], R. M. S. Schofield[47], E. Schreiber[8], D. Schuette[8], B. Schulz[8], B. F. Schutz[21,7], P. Schwinberg[25], J. Scott[26], S. M. Scott[64], F. Seifert[1], D. Sellers[6], A. S. Sengupta[120], D. Sentenac[23], A. Sergeev[99], D. Shaddock[64], S. Shah[87,9], M. S. Shahriar[79], M. Shaltev[8], B. Shapiro[29], P. Shawhan[51], D. H. Shoemaker[10], T. L. Sidery[20], K. Siellez[40], X. Siemens[12], D. Sigg[25], D. Simakov[8], A. Singer[1], L. Singer[1], A. M. Sintes[53], G. R. Skelton[12], B. J. J. Slagmolen[64], J. Slutsky[8], J. R. Smith[18], M. R. Smith[1], R. J. E. Smith[20], N. D. Smith-Lefebvre[1], K. Soden[12], E. J. Son[114], B. Sorazu[26], T. Souradeep[75], L. Sperandio[59,67], A. Staley[28], E. Steinert[25], J. Steinlechner[8], S. Steinlechner[8], S. Steplewski[43], D. Stevens[79], A. Stochino[64], R. Stone[34], K. A. Strain[26], N. Straniero[42], S. Strigin[36], A. S. Stroeer[34], R. Sturani[45,46], A. L. Stuver[6], T. Z. Summerscales[121], S. Susmithan[39], P. J. Sutton[7], B. Swinkels[23], G. Szeifert[82], M. Tacca[27], D. Talukder[47], L. Tang[34], D. B. Tanner[16], S. P. Tarabrin[8], R. Taylor[1], A. P. M. ter Braack[9], M. P. Thirugnanasambandam[1], M. Thomas[6], P. Thomas[25], K. A. Thorne[6], K. S. Thorne[62], E. Thrane[1], V. Tiwari[16], K. V. Tokmakov[108], C. Tomlinson[73], A. Toncelli[14,30], M. Tonelli[14,30], O. Torre[14,15], C. V. Torres[34], C. I. Torrie[1,26], F. Travasso[44,84], G. Traylor[6], M. Tse[28], D. Ugolini[122], C. S. Unnikrishnan[116], H. Vahlbruch[13], G. Vajente[14,30], M. Vallisneri[62], J. F. J. van den Brand[9,50], C. Van Den Broeck[9], S. van der Putten[9], M. V. van der Sluys[87,9], J. van Heijningen[9], A. A. van Veggel[26], S. Vass[1], M. Vasúth[74], R. Vaulin[10], A. Vecchio[20], G. Vedovato[123], J. Veitch[9], P. J. Veitch[92], K. Venkateswara[124], D. Verkindt[3], S. Verma[39], F. Vetrano[45,46], A. Viceré[45,46], R. Vincent-Finley[112], J.-Y. Vinet[40], S. Vitale[10,9], B. Vlcek[12], T. Vo[25], H. Vocca[44,84], C. Vorvick[25], W. D. Vousden[20], D. Vrinceanu[34], S. P. Vyachanin[36], A. Wade[64], L. Wade[12], M. Wade[12], S. J. Waldman[10], M. Walker[2], L. Wallace[1], Y. Wan[56], J. Wang[60], M. Wang[20], X. Wang[56], A. Wanner[8], R. L. Ward[64], M. Was[8], B. Weaver[25], L.-W. Wei[40], M. Weinert[8], A. J. Weinstein[1], R. Weiss[10], T. Welborn[6], L. Wen[39], P. Wessels[8], M. West[24], T. Westphal[8], K. Wette[8], J. T. Whelan[58], S. E. Whitcomb[1,39], D. J. White[73], B. F. Whiting[16], S. Wibowo[12], K. Wiesner[8], C. Wilkinson[25], L. Williams[16], R. Williams[1], T. Williams[125], J. L. Willis[126], B. Willke[8,13], M. Wimmer[8], L. Winkelmann[8], W. Winkler[8], C. C. Wipf[10], H. Wittel[8], G. Woan[26], J. Worden[25], J. Yablon[79], I. Yakushin[6], H. Yamamoto[1], C. C. Yancey[51], H. Yang[62], D. Yeaton-Massey[1], S. Yoshida[125], H. Yum[79], M. Yvert[3], A. Zadrożny[103], M. Zanolin[86], J.-P. Zendri[123], F. Zhang[10], L. Zhang[1], C. Zhao[39], H. Zhu[81], X. J. Zhu[39], N. Zotov[‡,117], M. E. Zucker[10], J. Zweizig[1]

The LIGO Scientific Collaboration & The Virgo Collaboration

S. Buchner[127,128], I. Cognard[129,130], A. Corongiu[131], N. D'Amico[131,132], C. M. Espinoza[133,134], P. C. C. Freire[135], E. V. Gotthelf[28], L. Guillemot[135], J. W. T. Hessels[136,137], G. B. Hobbs[138], M. Kramer[133,135], A. G. Lyne[133], F. E. Marshall[37], A. Possenti[131], S. M. Ransom[139], P. S. Ray[140], J. Roy[141], and B. W. Stappers[133]

Draft version April 25, 2014

ABSTRACT

We present the results of searches for gravitational waves from a large selection of pulsars using data from the most recent science runs (S6, VSR2 and VSR4) of the initial generation of interferometric gravitational wave detectors LIGO (Laser Interferometric Gravitational-wave Observatory) and Virgo. We do not see evidence for gravitational wave emission from any of the targeted sources but produce

upper limits on the emission amplitude. We highlight the results from seven young pulsars with large spin-down luminosities. We reach within a factor of five of the canonical spin-down limit for all seven of these, whilst for the Crab and Vela pulsars we further surpass their spin-down limits. We present new or updated limits for 172 other pulsars (including both young and millisecond pulsars). Now that the detectors are undergoing major upgrades, and, for completeness, we bring together all of the most up-to-date results from all pulsars searched for during the operations of the first-generation LIGO, Virgo and GEO600 detectors. This gives a total of 195 pulsars including the most recent results described in this paper.

Subject headings: gravitational waves - pulsars: general

[1] LIGO - California Institute of Technology, Pasadena, CA 91125, USA
[2] Louisiana State University, Baton Rouge, LA 70803, USA
[3] Laboratoire d'Annecy-le-Vieux de Physique des Particules (LAPP), Université de Savoie, CNRS/IN2P3, F-74941 Annecy-le-Vieux, France
[4] INFN, Sezione di Napoli, Complesso Universitario di Monte S.Angelo, I-80126 Napoli, Italy
[5] Università di Salerno, Fisciano, I-84084 Salerno, Italy
[6] LIGO - Livingston Observatory, Livingston, LA 70754, USA
[7] Cardiff University, Cardiff, CF24 3AA, United Kingdom
[8] Albert-Einstein-Institut, Max-Planck-Institut für Gravitationsphysik, D-30167 Hannover, Germany
[9] Nikhef, Science Park, 1098 XG Amsterdam, The Netherlands
[10] LIGO - Massachusetts Institute of Technology, Cambridge, MA 02139, USA
[11] Instituto Nacional de Pesquisas Espaciais, 12227-010 - São José dos Campos, SP, Brazil
[12] University of Wisconsin–Milwaukee, Milwaukee, WI 53201, USA
[13] Leibniz Universität Hannover, D-30167 Hannover, Germany
[14] INFN, Sezione di Pisa, I-56127 Pisa, Italy
[15] Università di Siena, I-53100 Siena, Italy
[16] University of Florida, Gainesville, FL 32611, USA
[17] The University of Mississippi, University, MS 38677, USA
[18] California State University Fullerton, Fullerton, CA 92831, USA
[19] INFN, Sezione di Roma, I-00185 Roma, Italy
[20] University of Birmingham, Birmingham, B15 2TT, United Kingdom
[21] Albert-Einstein-Institut, Max-Planck-Institut für Gravitationsphysik, D-14476 Golm, Germany
[22] Montana State University, Bozeman, MT 59717, USA
[23] European Gravitational Observatory (EGO), I-56021 Cascina, Pisa, Italy
[24] Syracuse University, Syracuse, NY 13244, USA
[25] LIGO - Hanford Observatory, Richland, WA 99352, USA
[26] SUPA, University of Glasgow, Glasgow, G12 8QQ, United Kingdom
[27] APC, AstroParticule et Cosmologie, Université Paris Diderot, CNRS/IN2P3, CEA/Irfu, Observatoire de Paris, Sorbonne Paris Cité, 10, rue Alice Domon et Léonie Duquet, F-75205 Paris Cedex 13, France
[28] Columbia University, New York, NY 10027, USA
[29] Stanford University, Stanford, CA 94305, USA
[30] Università di Pisa, I-56127 Pisa, Italy
[31] CAMK-PAN, 00-716 Warsaw, Poland
[32] INFN, Sezione di Genova, I-16146 Genova, Italy
[33] Università degli Studi di Genova, I-16146 Genova, Italy
[34] The University of Texas at Brownsville, Brownsville, TX 78520, USA
[35] San Jose State University, San Jose, CA 95192, USA
[36] Moscow State University, Moscow, 119992, Russia
[37] LAL, Université Paris-Sud, IN2P3/CNRS, F-91898 Orsay, France
[38] NASA/Goddard Space Flight Center, Greenbelt, MD 20771, USA
[39] University of Western Australia, Crawley, WA 6009, Australia
[40] Université Nice-Sophia-Antipolis, CNRS, Observatoire de la Côte d'Azur, F-06304 Nice, France
[41] Institut de Physique de Rennes, CNRS, Université de Rennes 1, F-35042 Rennes, France
[42] Laboratoire des Matériaux Avancés (LMA), IN2P3/CNRS, Université de Lyon, F-69622 Villeurbanne, Lyon, France
[43] Washington State University, Pullman, WA 99164, USA
[44] INFN, Sezione di Perugia, I-06123 Perugia, Italy
[45] INFN, Sezione di Firenze, I-50019 Sesto Fiorentino, Firenze, Italy
[46] Università degli Studi di Urbino 'Carlo Bo', I-61029 Urbino, Italy
[47] University of Oregon, Eugene, OR 97403, USA
[48] Laboratoire Kastler Brossel, ENS, CNRS, UPMC, Université Pierre et Marie Curie, F-75005 Paris, France
[49] Astronomical Observatory Warsaw University, 00-478 Warsaw, Poland
[50] VU University Amsterdam, 1081 HV Amsterdam, The Netherlands
[51] University of Maryland, College Park, MD 20742, USA
[52] University of Massachusetts - Amherst, Amherst, MA 01003, USA
[53] Universitat de les Illes Balears, E-07122 Palma de Mallorca, Spain
[54] Università di Napoli 'Federico II', Complesso Universitario di Monte S.Angelo, I-80126 Napoli, Italy
[55] Canadian Institute for Theoretical Astrophysics, University of Toronto, Toronto, Ontario, M5S 3H8, Canada
[56] Tsinghua University, Beijing 100084, China
[57] University of Michigan, Ann Arbor, MI 48109, USA
[58] Rochester Institute of Technology, Rochester, NY 14623, USA
[59] INFN, Sezione di Roma Tor Vergata, I-00133 Roma, Italy
[60] National Tsing Hua University, Hsinchu Taiwan 300
[61] Charles Sturt University, Wagga Wagga, NSW 2678, Australia
[62] Caltech-CaRT, Pasadena, CA 91125, USA
[63] Pusan National University, Busan 609-735, Korea
[64] Australian National University, Canberra, ACT 0200, Australia
[65] Carleton College, Northfield, MN 55057, USA
[66] INFN, Gran Sasso Science Institute, I-67100 L'Aquila, Italy
[67] Università di Roma Tor Vergata, I-00133 Roma, Italy
[68] Università di Roma 'La Sapienza', I-00185 Roma, Italy
[69] University of Sannio at Benevento, I-82100 Benevento, Italy and INFN (Sezione di Napoli), Italy
[70] The George Washington University, Washington, DC 20052, USA
[71] University of Cambridge, Cambridge, CB2 1TN, United Kingdom
[72] University of Minnesota, Minneapolis, MN 55455, USA
[73] The University of Sheffield, Sheffield S10 2TN, United Kingdom
[74] Wigner RCP, RMKI, H-1121 Budapest, Konkoly Thege Miklós út 29-33, Hungary
[75] Inter-University Centre for Astronomy and Astrophysics, Pune - 411007, India
[76] INFN, Gruppo Collegato di Trento, I-38050 Povo, Trento, Italy
[77] Università di Trento, I-38050 Povo, Trento, Italy
[78] California Institute of Technology, Pasadena, CA 91125, USA
[79] Northwestern University, Evanston, IL 60208, USA
[80] Montclair State University, Montclair, NJ 07043, USA
[81] The Pennsylvania State University, University Park, PA 16802, USA
[82] MTA-Eotvos University, 'Lendulet'A. R. G., Budapest 1117, Hungary
[83] National Astronomical Observatory of Japan, Tokyo 181-8588, Japan
[84] Università di Perugia, I-06123 Perugia, Italy
[85] Rutherford Appleton Laboratory, HSIC, Chilton, Didcot, Oxon, OX11 0QX, United Kingdom
[86] Embry-Riddle Aeronautical University, Prescott, AZ 86301, USA

1. INTRODUCTION

Pulsars are spinning, magnetized neutron stars with slowly decreasing rotation rates. In the model of a triaxial ellipsoid star, a deformation (possibly from shear strains in the solid part(s) of the star, or from magnetic stresses) can appear as a time-varying quadrupole moment as the star rotates. The observed loss of rotational energy, known as the spin-down luminosity (given by $\dot{E} = I_{zz}\Omega|\dot{\Omega}| = 4\pi^2 I_{zz} f_{\rm rot}|\dot{f}_{\rm rot}|$, where I_{zz} is the moment of inertia around the principal axis (aligned with the rotation axis), $f_{\rm rot}$ is the rotation frequency, and $\dot{f}_{\rm rot}$ is the rotational frequency derivative) provides a huge reservoir of energy. Along with magnetic dipole radiation some fraction of this reservoir is potentially dissipated through gravitational wave emission (see Shklovskii 1969; Ostriker & Gunn 1969; Ferrari & Ruffini 1969; Melosh 1969 for four contemporaneous calculations of gravitational wave emission from soon after pulsars were discovered, or e.g. Owen 2006 for a review of more recent emission mechanism calculations). Known pulsars usually have precisely determined frequency evolutions and sky-positions making them ideal targets for gravitational wave detectors. If a pulsar is monitored regularly through electromagnetic observations it can yield a coherent phase model, which allows gravitational wave data to be coherently integrated over months or years.

Since the initial science data runs of the Laser Interferometric Gravitational-wave Observatory (LIGO), Virgo and GEO600, searches have been performed for continuous quasi-monochromatic gravitational wave emission from many known pulsars (Abbott et al. 2004, 2005, 2007b, 2008, 2010; Abadie et al. 2011). Most recently 116 known pulsars were targeted using data from LIGO's fifth science run (S5 Abbott et al. 2010), and the Vela pulsar (J0835−4510) was targeted using data from Virgo's second science run (VSR2). These searches reported no detections, but provided upper limits on the gravitational wave amplitude from the sources and surpassed the so-called spin-down limit (see Section 1.1) for the Crab and Vela pulsars.

We aim here to search for gravitational wave emission from a large selection of stars including some of those with the largest spin-down luminosities. Due to the sensitivity reduction caused at low frequency by seismic noise at the detectors, it is not worthwhile to search for pulsars with rotational frequencies, $f_{\rm rot}$, smaller than about 10 Hz, which corresponds to gravitational wave mass quadrupole emission at frequencies, $f_{\rm gw} = 2f_{\rm rot}$, smaller than 20 Hz. The exact value of this gravitational wave low-frequency cut-off is rather arbitrary, our choice of taking 20 Hz is motivated by the presence of several noise lines and bumps in Virgo data at lower frequencies. In general, young pulsars, with large spin-down luminosities are searched for at lower frequencies where the Virgo detector has better sensitivity, whereas the search for

[87] Department of Astrophysics/IMAPP, Radboud University Nijmegen, P.O. Box 9010, 6500 GL Nijmegen, The Netherlands
[88] Perimeter Institute for Theoretical Physics, Ontario, N2L 2Y5, Canada
[89] American University, Washington, DC 20016, USA
[90] University of New Hampshire, Durham, NH 03824, USA
[91] College of William and Mary, Williamsburg, VA 23187, USA
[92] University of Adelaide, Adelaide, SA 5005, Australia
[93] Raman Research Institute, Bangalore, Karnataka 560080, India
[94] Korea Institute of Science and Technology Information, Daejeon 305-806, Korea
[95] Białystok University, 15-424 Białystok, Poland
[96] University of Southampton, Southampton, SO17 1BJ, United Kingdom
[97] IISER-TVM, CET Campus, Trivandrum Kerala 695016, India
[98] Hobart and William Smith Colleges, Geneva, NY 14456, USA
[99] Institute of Applied Physics, Nizhny Novgorod, 603950, Russia
[100] Seoul National University, Seoul 151-742, Korea
[101] Hanyang University, Seoul 133-791, Korea
[102] IM-PAN, 00-956 Warsaw, Poland
[103] NCBJ, 05-400 Świerk-Otwock, Poland
[104] Institute for Plasma Research, Bhat, Gandhinagar 382428, India
[105] Utah State University, Logan, UT 84322, USA
[106] The University of Melbourne, Parkville, VIC 3010, Australia
[107] University of Brussels, Brussels 1050 Belgium
[108] SUPA, University of Strathclyde, Glasgow, G1 1XQ, United Kingdom
[109] ESPCI, CNRS, F-75005 Paris, France
[110] Università di Camerino, Dipartimento di Fisica, I-62032 Camerino, Italy
[111] The University of Texas at Austin, Austin, TX 78712, USA
[112] Southern University and A&M College, Baton Rouge, LA 70813, USA
[113] IISER-Kolkata, Mohanpur, West Bengal 741252, India
[114] National Institute for Mathematical Sciences, Daejeon 305-390, Korea
[115] RRCAT, Indore MP 452013, India
[116] Tata Institute for Fundamental Research, Mumbai 400005, India
[117] Louisiana Tech University, Ruston, LA 71272, USA
[118] SUPA, University of the West of Scotland, Paisley, PA1 2BE, United Kingdom
[119] Institute of Astronomy, 65-265 Zielona Góra, Poland
[120] Indian Institute of Technology, Gandhinagar Ahmedabad Gujarat 382424, India
[121] Andrews University, Berrien Springs, MI 49104, USA
[122] Trinity University, San Antonio, TX 78212, USA
[123] INFN, Sezione di Padova, I-35131 Padova, Italy
[124] University of Washington, Seattle, WA 98195, USA
[125] Southeastern Louisiana University, Hammond, LA 70402, USA
[126] Abilene Christian University, Abilene, TX 79699, USA
[127] Hartebeesthoek Radio Astronomy Observatory, PO Box 443, Krugersdorp, 1740, South Africa
[128] School of Physics, University of the Witwatersrand, Johannesburg, South Africa
[129] LPC2E/CNRS-Université d'Orléans, 45071 Orléans, France
[130] Nançay/Paris Observatory, 18330 Nançay, France
[131] INAF - Osservatorio Astronomico di Cagliari, Poggio dei Pini, 09012 Capoterra, Italy
[132] Dipartimento di Fisica Università di Cagliari, Cittadella Universitaria, I-09042 Monserrato, Italy
[133] Jodrell Bank Centre for Astrophysics, School of Physics and Astronomy, University of Manchester, Manchester M13 9PL, UK
[134] Instituto de Astrofísica, Facultad de Física, Pontificia Universidad Católica de Chile, Casilla 306, Santiago 22, Chile
[135] Max-Planck-Institut für Radioastronomie, Auf dem Hügel 69, D-53121 Bonn, Germany
[136] ASTRON, the Netherlands Institute for Radio Astronomy, Postbus 2, 7990 AA, Dwingeloo, The Netherlands
[137] Astronomical Institute "Anton Pannekoek", University of Amsterdam, Science Park 904, 1098 XH Amsterdam, The Netherlands
[138] Australia Telescope National Facility, CSIRO, PO Box 76, Epping NSW 1710, Australia
[139] National Radio Astronomy Observatory, Charlottesville, VA 22903, USA
[140] Space Science Division, Naval Research Laboratory, Washington, DC 20375-5352, USA
[141] National Centre for Radio Astrophysics, Pune 411007, India
[†] Deceased, April 2012.
[‡] Deceased, May 2012.

millisecond pulsars (MSPs) is conducted at higher frequencies where the LIGO detectors are more sensitive. The selection of pulsars will be discussed more fully in Section 2.

1.1. *The signal*

The expected quadrupolar gravitational wave signal from a triaxial neutron star[144] steadily spinning about one of its principal axes of inertia is at twice the rotation frequency, with a strain of

$$\begin{aligned} h(t) =& \frac{1}{2}F_+(t,\psi)h_0(1+\cos^2\iota)\cos\phi(t) \\ &+ F_\times(t,\psi)h_0\cos\iota\sin\phi(t) \end{aligned} \quad (1)$$

in the detector, where

$$h_0 = \frac{16\pi^2 G}{c^4}\frac{I_{zz}\varepsilon f_{\rm rot}^2}{d} \quad (2)$$

is the dimensionless gravitational wave strain amplitude. h_0 is dependent on I_{zz}, the fiducial equatorial ellipticity, defined as $\varepsilon = \frac{I_{xx}-I_{yy}}{I_{zz}}$ in terms of principal moments of inertia, the rotational frequency, $f_{\rm rot}$, and the distance to the source d. The signal amplitudes in the two polarizations ('+' and '×') depend on the inclination of the star's rotation axis to the line-of-sight, ι, while the detector antenna pattern responses for the two polarization states, $F_+(t,\psi)$ and $F_\times(t,\psi)$, depend on the gravitational wave polarization angle, ψ, as well as the detector location, orientation and source sky position. The gravitational wave phase evolution, $\phi(t)$, depends on both the intrinsic rotational frequency and frequency derivatives of the pulsar and on Doppler and propagation effects. These extrinsic effects include relativistic modulations caused by the Earth's orbital and rotational motion, the presence of massive bodies in the solar system close to the line-of-sight to the pulsar, the proper motion of the pulsar, and (in the case of a binary system) pulsar orbital motions. We will assume that $\phi(t)$ is phase-locked to the electromagnetic pulse phase evolution, but with double the value and with an initial phase offset, ϕ_0. Given this phase evolution, the four unknown search parameters are simply h_0, $\cos\iota$, ϕ_0 and ψ. The gravitational wave amplitude is related to the star's $l = m = 2$ mass quadrupole moment via (see e.g. Owen 2005)

$$Q_{22} = \sqrt{\frac{15}{8\pi}}I_{zz}\varepsilon = h_0\left(\frac{c^4 d}{16\pi^2 G f_{\rm rot}^2}\right)\sqrt{\frac{15}{8\pi}}, \quad (3)$$

where Q_{22} is the slightly non-standard definition of quadrupole moment used in Ushomirsky et al. (2000) and many subsequent papers. This value can be constrained independently of any assumptions about the star's equation of state and moment of inertia.

If we allocate all the spin-down luminosity, $\dot{E}$, to gravitational wave luminosity, $\dot{E}_{\rm gw}$, where

$$\begin{aligned} \dot{E}_{\rm gw} =& \frac{2048\pi^6}{5}\frac{G}{c^5}f_{\rm rot}^6(I_{zz}\varepsilon)^2, \\ =& \frac{8\pi^2}{5}\frac{c^3}{G}f_{\rm rot}^2 h_0^2 d^2, \end{aligned} \quad (4)$$

then we have the canonical 'spin-down limit' on gravitational wave strain[145]

$$\begin{aligned} h_0^{\rm sd} &= \left(\frac{5}{2}\frac{GI_{zz}\dot{f}_{\rm rot}}{c^3 d^2 f_{\rm rot}}\right)^{1/2} \\ &= 8.06\times10^{-19}\frac{I_{38}^{1/2}}{d_{\rm kpc}}\left(\frac{|\dot{f}_{\rm rot}|}{f_{\rm rot}}\right)^{1/2}, \end{aligned} \quad (5)$$

where I_{38} is the star's moment of inertia in the units of $10^{38}\,{\rm kg\,m^2}$, and $d_{\rm kpc}$ is the distance to the pulsar in kiloparsecs. The spin-down limit on the signal amplitude corresponds (via equation 2) to an upper limit on the star's fiducial ellipticity[146]

$$\varepsilon^{\rm sd} = 0.237\left(\frac{h_0^{\rm sd}}{10^{-24}}\right)f_{\rm rot}^{-2}I_{38}^{-1}d_{\rm kpc}. \quad (6)$$

Johnson-McDaniel (2013) shows how to relate this to the physical ellipticity of the star's surface for a given equation of state.

A gravitational wave strain upper limit that is below the spin-down limit is an important milestone, as such a measurement is probing uncharted regions of the parameter space. Likewise it directly constrains the fraction of spin-down power that could be due to the emission of gravitational waves, which gives insight into the overall spin-down energy budget.

1.2. *The science runs*

In this paper we have used calibrated data from the Virgo second (Aasi et al. 2012) and fourth science runs (VSR2 and VSR4) and the LIGO sixth science run (S6). Virgo's third science run (VSR3) was relatively insensitive in comparison with VSR4 and has not been included in this analysis. This was partially because Virgo introduced monolithic mirror suspensions prior to VSR4 which improved sensitivity in the low-frequency range. During S6, the two LIGO 4 km detectors at Hanford, Washington (LHO/H1), and Livingston, Louisiana (LLO/L1), were running in an enhanced configuration (Adhikari et al. 2006) over that from the previous S5 run (Abbott et al. 2009). Table 1 shows dates of the runs, the duty factors and science data lengths for each detector that we analyzed.

The Virgo and LIGO data used in these analyses have been calibrated through different reconstruction proce-

[144] We use 'triaxial neutron star' as shorthand for a star with some asymmetry with respect to its rotation axis and therefore a triaxial moment of inertia ellipsoid.

[145] As noted in Johnson-McDaniel (2013), the versions of this equation given inline in the first paragraph of Abbott et al. (2008), as equation (1) in Abbott et al. (2010) and as equation (14) in Abadie et al. (2011) are incorrect and should have I_{38} substituted for $I_{38}^{1/2}$.

[146] Again, as noted in Johnson-McDaniel (2013), the versions of this equation given inline in Section 3 of Abbott et al. (2008) and as equation (7) in Abbott et al. (2010) are incorrect and should have I_{38} substituted for I_{38}^{-1}.

TABLE 1
SCIENCE RUNS.

Run	Dates	Duty factor (%)	Data length (days)
VSR2	2009 Jul 7 (20:55 UTC) – 2010 Jan 8 (22:00 UTC)	80.4	149
VSR4	2011 Jun 3 (10:27 UTC) – 2011 Sep 5 (13:26 UTC)	81.0	76
S6 Hanford (H1)	2009 Jul 7 (21:00 UTC) – 2010 Oct 21 (00:00 UTC)	50.6	238
S6 Livingston (L1)	2009 Jul 7 (21:00 UTC) – 2010 Oct 21 (00:00 UTC)	47.9	225

dures, but both based ultimately on the measured response to actuation controls on the positions of the mirrors that define the interferometers. For Virgo VSR2, the calibration uncertainty was about 5.5% in amplitude and ∼50 mrad (3°) in phase over most of the frequency range (Accadia et al. 2011). For VSR4, the uncertainty amounted to about 7.5% in amplitude and to $(40 + 50f)$ mrad in phase, where f is the frequency in kilohertz, for frequencies up to 500 Hz (Mours & Rolland 2011). For LIGO, the S6 calibration uncertainties over the relevant frequency range (50–1500 Hz) were up to ∼19% in amplitude and ∼170 mrad (10°) in phase for L1, and up to ∼16% in amplitude and ∼120 mrad (7°) for H1 (Bartos et al. 2011). These phase errors are well within the range (i.e. less than 30°as applied in Abbott et al. 2007b) that would cause significant loss in signal power due to decoherence between the pulsar signal and the assumed phase evolution.

1.3. *Methods*

We used three semi-independent methods (very similar to those used in the Vela pulsar search in Abadie et al. 2011) to search for signals described in Section 1.1. Here, we briefly outline their operation, but for full descriptions we refer the reader to the references below. Two of the search methods work with time domain data that has been heterodyned to remove the signal's phase evolution and then heavily decimated. This leaves a complex data stream in which any signal would only be modulated by the detector's beam pattern. In the first method, this data stream is used to give Bayesian parameter estimates of the unknown signal parameters[147] (Dupuis & Woan 2005). The second method computes the maximum likelihood $\mathcal{F}$-statistic rather than a Bayesian posterior (or in case where ψ and ι are well constrained, the $\mathcal{G}$-statistic) (Jaranowski & Królak 2010). The third method (Astone et al. 2010) makes use of a Short Fourier Transform Database (SFDB) of each detector's data. After the extraction of a small frequency band around the signal's expected frequency, the Doppler effect, Einstein delay and spin-down are removed in the time domain and the data are down-sampled with a re-sampling technique. Two matched filters on the '+' and '×' signal Fourier components are then computed at the five frequencies at which the signal power is spread due to the signal amplitude and phase modulation; they are used to build a detection statistic and to estimate signal parameters in the case of detection. This 5-vector method has been extended over that used in Abadie et al. (2011) to allow for coherent analysis of data from multiple detectors (Astone et al. 2012). Each of these methods can incorporate prior information on the pulsar's inclination and polarization angle. From here on, we will refer to the first method as the *Bayesian* method[148], the second as the *$\mathcal{F}/\mathcal{G}$-statistic* method and the third as the *$5n$-vector* method, where n refers to the number of datasets coherently combined.

All three methods apply some data cleaning. The procedure used to obtain the heterodyned data removes extreme outliers by running two passes of a scheme that identifies points with absolute values greater than five times the standard deviation of the dataset. The $\mathcal{F}/\mathcal{G}$-statistic method performs further cleaning of this data through the Grubbs test (see Abadie et al. 2011). In the $5n$-vector method, after an initial time-domain cleaning before the construction of the SFDB, a further cleaning step is applied on the final down-sampled time series in which the largest outliers belonging to the non-Gaussian tail of the data amplitude distribution are removed.

We have incorporated some limits from the previous LIGO S5 results (Abbott et al. 2010) as priors in the Bayesian analysis. However, the S6/VSR2,4 phase models were produced with updated pulsar ephemerides resulting in an unknown phase offset between them and the S5 results. We have, therefore, simply used the S5 marginalised posterior on h_0 and $\cos\iota$, $p(h_0, \cos\iota)$, as our prior for the new results. In the case of glitching pulsars (see Section 2), we used the same approach and (incoherently) combined the separate coherent analyses produced between glitches. In the case of the $\mathcal{F}/\mathcal{G}$-statistic method, the results from different detectors or different inter-glitch periods are combined incoherently by adding the respective statistics. Also, for the $5n$-vector method, results from different inter-glitch periods are incoherently combined by summing the corresponding statistics. Our reasons for not coherently combining the data over glitches are twofold. The first is that we do not know how a glitch would effect the relative phase offset between the electromagnetic pulses and the gravitational wave signal. The second reason is a practical consideration based on the timing solutions we have for our pulsars. For three of the four glitching pulsars (all except J0537−6910) in this analysis we have separate timing solutions for each inter-glitch period. These separate timing solutions, as provided by the pulsar timing software TEMPO(2), do not give an epoch defined at a fixed pulse phase (i.e. the epoch is not given as the time of the peak of a particular pulse), so there is some unknown phase offset between the separate solutions. However, if this phase offset were

[147] For this analysis the parameter posterior distributions were recreated using a Markov chain Monte Carlo (Abbott et al. 2010). For each pulsar five independent chains were produced with 50 000 burn-in samples and 200 000 posterior samples in each. The chains were thinned using the autocorrelation length to give uncorrelated samples, and to test for convergence, the chains were then examined by eye, and a Gelman-Rubins test was performed (see e.g. Brooks & Roberts 1998).

[148] For this analysis, the results were produced with version 6.16 of the LSC Algorithm Library Suite (LALSuite) `https://www.lsc-group.phys.uwm.edu/daswg/projects/lalsuite.html`.

known (e.g. by going back to the original pulsar pulse time of arrival data) the gain in sensitivity would still be minimal: for the Vela pulsar and J1813−1246 the data from VSR4 (which was after the glitches in these pulsars) was much more sensitive, so completely dominates the result; for J1952+3252 the post-glitch data contains the latter part of S6, which was more sensitive and would again dominate the results. For J0537−6910 the epoch for each inter-glitch timing solution is defined (see Table 6), so the electromagnetic phase could be tracked over the glitches, but again our result is dominated by the longest and most sensitive inter-glitch period.

Even without a detection, all three methods can be used to produce upper limits on the gravitational wave amplitude from the pulsars. Here, we will quote 95% confidence upper limits on the amplitude. In the Bayesian method, an upper limit on the h_0 posterior (after marginalization over the orientation parameters) is found by calculating the upper bound, from zero, on the integral over this posterior that encloses 95% of the probability. In the $\mathcal{F}/\mathcal{G}$-statistic method, a frequentist upper limit is calculated through Monte-Carlo simulations, which find the value of h_0 for which 95% of trials exceed the maximum likelihood statistic[149]. The $5n$-vector method computes an upper limit on the H_0 posterior, given the actual value of the detection statistic, and the marginalization over the other parameters is implicitly done in the Monte Carlo simulation used to compute the likelihood. The amplitude, H_0, is linked to the classical h_0, given by equation 2, by the relation $H_0 = \frac{h_0}{2}\sqrt{1+6\cos^2\iota+\cos^4\iota}$ (see equation (A5) in Abadie et al. 2011). H_0 is the strain amplitude of a linearly polarized signal with polarization angle $\psi = 0$. In order to convert an upper limit on H_0 to an upper limit on h_0, we use the previous equation replacing the coefficient on the right hand side with its mean value over the distribution of $\cos\iota$ used in the upper limit procedure. This is justified by the fact that the posterior distribution of H_0 is not dependent on ι. The three methods have been tested with hardware and software simulated signal injections to check that they can recover the expected signal model (see e.g. Abadie et al. 2011). In the Bayesian analysis these upper limits are really 95% credibility, or degrees-of-belief, values, whereas for the frequentist analysis these are 95% confidence values. These are both asking different questions and in general should not be expected to produce identical results. A brief discussion of this is given in the first search for a pulsar in LIGO data in Abbott et al. (2004), whilst a more technical discussion of the differences between the upper limits can be found in Röver et al. (2011).

2. PULSAR SELECTION

The sensitivity of the Virgo and LIGO detectors allows us to target pulsars with $f_{\rm rot} > 10\,$Hz. Currently the Australia Telescope National Facility (ATNF) pulsar catalog (Manchester et al. 2005) contains data for 368 pulsars (out of a total of 2264) consistent with this criterion[150]. The majority of these (∼90%) are recycled MSPs that have been spun-up to high rotation frequencies by accretion from a binary companion which may still be present (see e.g. Lorimer 2008, for an overview of MSPs and binary pulsars). MSPs spin down slowly (with $\dot{f}_{\rm rot}$ between approximately -10^{-14} and $-10^{-17}\,$Hz/s) and have characteristic ages[151] greater than a few times 10^8 years, implying a comparatively weak surface polar magnetic field ($10^8 \lesssim B_s \lesssim 10^9\,$G, via the relation for an orthogonal rotator with radius 10 km and $I_{zz} = I_{38}$ of $B_s = 3.3\times10^{19}(|\dot{f}_{\rm rot}|/f_{\rm rot}^3)^{1/2}\,$G) compared to "normal" pulsars. About 10% are young pulsars with $\dot{f}_{\rm rot}$ between approximately -10^{-10} and $-10^{-12}\,$Hz/s, characteristic ages of between ∼1000 and a few tens of thousands of years, and therefore with the large implied surface magnetic fields of "normal" pulsars, $B_s \sim 10^{12}\,$G. They are situated towards the low-frequency end of our sensitivity range.

Young pulsars have large spin-downs and relatively low frequencies, so in general have the highest gravitational wave spin-down limits, see equation 5. This makes them particularly important targets as the limits can be within reach of current detectors. Equations 3 and 6 show that to produce emission at around the spin-down limit the required mass quadrupole/ellipticity would have to be large, at a level consistent with only the most exotic neutron star equations of state (see the discussion in Section 4). Such strong emission is unlikely, but its detection would have profound implications. Young pulsars also often show rotational anomalies such as glitches and timing noise (see e.g. Helfand et al. 1980). The underlying causes of such phenomena are still quite uncertain, and gravitational wave data would be a powerful constraint. For the MSPs, the spin-down limits are generally several orders of magnitude below those for the young pulsars. They are located, however, in a more sensitive frequency range.

2.1. *Electromagnetic pulsar observations*

For this analysis, we have obtained ephemerides using radio, X-ray and γ-ray observations. The radio telescope observations have come from a variety of sources: the 12.5-m telescope and Lovell telescope at Jodrell Bank in the UK, the 26-m telescope at Hartebeesthoek in South Africa, the 15-m eXperimental Development Model (XDM) telescope in South Africa, the Giant Metrewave Radio Telescope (GMRT) in India, the Robert C. Byrd Green Bank Radio Telescope (GBT) in the US, the Parkes radio telescope in Australia, the Nançay Decimetric Radio Telescope in France and the Hobart radio telescope in Australia. High energy X-ray and γ-ray timings have been obtained from the Rossi X-ray Timing Explorer (RXTE) and the *Fermi* Large Area Telescope (LAT).

In total, for this analysis, we collected timing solutions for 179 pulsars. This selection includes 73 pulsars that

[149] The $\mathcal{F}/\mathcal{G}$-statistic is most suitable for signal detection, whilst the upper limit derived from it here is mainly given for completeness. In the future a more sophisticated method, such as that of Feldman & Cousins (1998), may be used to produce frequentist confidence intervals for this analysis.

[150] ATNF pulsar catalog v1.47 `http://www.atnf.csiro.au/people/pulsar/psrcat/`

[151] Characteristic age is given by $\tau = -(1/(n-1))(f_{\rm rot}/\dot{f}_{\rm rot})$, which, for a magnetic dipole braking index of $n = 3$, gives $\tau = -f_{\rm rot}/(2\dot{f}_{\rm rot})$, and for purely gravitational wave (quadrupole) spin-down would be $n = 5$, giving $\tau = -f_{\rm rot}/(4\dot{f}_{\rm rot})$ (a "gravitar", Palomba 2005; Knispel & Allen 2008).

TABLE 2
Electromagnetic observation epochs for the high interest pulsars.

MJD and date
J0534+2200 (Crab pulsar)
54997 (2009 Jun 15) – 55814 (2011 Sep 10)
J0537−6910 (N157B)
54897 (2009 Mar 7) – 55041 (2009 Jul 29)
55045 (2009 Aug 2) – 55182 (2009 Dec 17)
55185 (2009 Dec 20) – 55263 (2010 Mar 8)
55275 (2010 Mar 20) – 55445 (2010 Sep 6)
55458 (2010 Sep 19) – 55503 (2010 Nov 3)
J0835−4510 (Vela pulsar)
54983 (2009 Jun 1) – 55286 (2010 Mar 31)
55713 (2011 Jun 1) – 55827 (2011 Sep 23)
J1813−1246
54693 (2008 Aug 15) – 55094 (2009 Sep 20)
55094 (2009 Sep 20) – 55828 (2011 Sep 24)
J1833−1034 (G21.5−0.9)
55041 (2009 Jul 29) – 55572 (2011 Jan 11)
J1913+1011
54867 (2009 Feb 5) – 55899 (2011 Dec 4)
J1952+3252 (CTB 80)
54589 (2008 May 3) – 55325 (2010 May 9)
55331 (2010 May 15) – 55802 (2011 Aug 29)

have not been previously studied. However, for five of the pulsars targeted in the S3/S4 analysis (Abbott et al. 2007b) and another eleven of the pulsars targeted in the S5 analysis (Abbott et al. 2010), new coherent timing solutions were not available, so these stars[152] have not been included in this search.

2.1.1. *High interest targets*

As discussed in Abbott et al. (2008)[153], due to our ignorance of the correct neutron star equation of state there is a large uncertainty in the moments of inertia for our targets, from 1 to $3\times10^{38}\,\mathrm{kg\,m^2}$. Therefore, the canonical spin-down limit estimates could be increased by a factor of ∼1.7. Also, there are uncertainties in some pulsar distance measurements of up to a factor of two which could further increase or decrease the spin-down limit. We therefore identified all sources that were within a factor of four of the canonical spin-down limit as worthy of special attention. Seven of the pulsars for which we have obtained timing solutions beat, or approach to within a factor of four, this limit. The electromagnetic observation epochs for each pulsar (which include each inter-glitch epoch for pulsars that glitched during the analysis) are given in Table 2. Further details of these observations are given below:

J0534+2200 (the Crab pulsar) We have used the Jodrell Bank Monthly Ephemeris (Lyne et al. 1993) to track the phase of the Crab pulsar over the period of our runs. This ephemeris has timing solutions using the DE200 solar system ephemeris and the TDB time coordinate system. During S6/VSR2,4 the pulsar did not show signs of any timing glitches.

J0537−6910 (N157B) Long-term X-ray timing has been performed with the RXTE (Middleditch et al. 2006). Recent data covering S6 shows four glitches over the span of our science runs and the ephemerides for each inter-glitch epoch are given in Appendix A. The timing solutions used the DE200 solar system ephemeris (see Marshall et al. 1998) and the TDB time coordinate system. Several more glitches have been observed since the end of our science runs, but we do not report on them here.

J0835−4510 (the Vela pulsar) Radio observations over the period of VSR2 were taken with the Hobart radio telescope in Tasmania and the Hartebeesthoek 26-m radio telescope in South Africa (Abadie et al. 2011). Radio timing over the VSR4 run was performed with the XDM telescope and the 26-m telescope at Hartebeesthoek. The timing solutions have used the DE405 solar system ephemeris and the TCB time coordinate system. Vela was observed to glitch on 2010 July 31 (Buchner 2010), between VSR2 and VSR4, but it has not glitched since then.

J1813−1246 This pulsar was discovered in a search of gamma-ray data from the *Fermi* LAT (Abdo et al. 2009), and using the unbinned maximum likelihood methods of Ray et al. (2011) timing measurements were made covering all our runs. It was observed to glitch once during this time on 2009 September 20. Pre-and-post glitch timing solutions have been produced using the DE405 solar system ephemeris and the TDB time coordinate system.

J1833−1034 (G21.5−0.9) The period from the start of S6/VSR2 until 2011 January is covered by observations made with the Giant Metrewave Radio Telescope (GMRT) (Roy et al. 2012). During this period, one glitch was observed, with a best fit epoch of 2009 November 6 (MJD 55142±2). To remove its effect, an ephemeris fit was performed on timing data excluding 80 days after the glitch. The timing solution uses the DE405 solar system ephemeris and the TDB time coordinate system.

J1913+1011 This pulsar was observed at Jodrell Bank and showed no timing anomalies over the science runs. The timing solution uses the DE405 solar system ephemeris and the TDB time coordinate system.

J1952+3252 (CTB 80) This pulsar was observed over the whole of our science runs at Nançay and Jodrell Bank. It glitched on 2010 May 11 (MJD

[152] The five additional pulsars targeted in S3/S4 were J1435−6100, J1629−6902, J1757−5322, J1911+0101A and J1911+0101B and the eleven additional pulsars targeted in S5 were J1701−3006B, J1701−3006C, J1748−2446P, J1748−2446ad, J1824−2452B, J1824−2452C, J1824−2452E, J1824−2452F, J1824−2452G, J1824−2452H, J1824−2452J.

[153] Note that Johnson-McDaniel (2013) computes even larger potential moments of inertia at $\sim5\times10^{38}\,\mathrm{kg\,m^2}$ for some solid quark stars.

TABLE 3
Implied orientations of pulsars from their pulsar wind nebulae observations (Ng & Romani 2004, 2008).

Pulsar	ι	ψ
J0534+2200 (Crab pulsar)	$62°.2 \pm 1°.9$	$35°.2 \pm 1°.5$
J0537−6910	$92°.8 \pm 0°.9$	$41°.0 \pm 2°.2$
J0835-4510 (Vela pulsar)	$63°.6 \pm 0°.6$	$40°.6 \pm 0°.1$
J1833−1034	$85°.4 \pm 0°.3$	$45° \pm 1°$
J1952+3252†	···	$-11°.5 \pm 8°.6$

† The polarization angle is not taken from a fit to the pulsar wind nebula, but instead is the average of the angle calculated from proper motion measurements and Hα observations of a bow shock (Ng & Romani 2004).

55327), between the end of S6/VSR2 and the start of VSR4. Phase incoherent pre- and post-glitch timing solutions have been produced using the DE405 solar system ephemeris and the TCB time ephemeris. The solution include fits to the timing noise using the TEMPO2 FITWAVES method described in Hobbs et al. (2006).

For several of these pulsars potential constraints on their orientations (the inclination ι and polarization angle ψ[154]) are available from observations of their pulsar wind nebulae (Ng & Romani 2004, 2008). These are listed in Table 3 where the uncertainties used are estimated from the systematic and statistical values given in Ng & Romani (2004, 2008), and the mean angle value is used if multiple fits are given (e.g. fits to the inner and outer tori of the Crab pulsar wind nebula). We briefly discussed how these constraints are used in the analyses in Section 1.3.

For J0534+2200 and J0537−6910, the Bayesian method also makes use of results from the LIGO S5 run (Abbott et al. 2010) as a prior on the h_0 and $\cos\iota$ parameters. During S5, both of these pulsars glitched, and the data for each inter-glitch period was analyzed independently. Results were also produced assuming that the data could be analyzed coherently over the glitches. To avoid the assumptions about coherence over the glitches, we have used the independent inter-glitch results that gave the lowest h_0 as the prior for the current analysis (see Table 3 of Abbott et al. 2010).

3. RESULTS

None of the searches yielded evidence of a gravitational wave signal, and upper limits have been placed on signal strengths. These limits are subject to the uncertainties in the amplitude calibration, as discussed in Section 1.2. For the joint results, which combine data from multiple detectors, the sensitivity is often dominated by the most sensitive instrument. Therefore, we expect the amplitude uncertainty due to calibration uncertainties to also be dominated by the most sensitive instrument. So, following the calibration error given in Section 1.2, below ∼50 Hz we have an amplitude uncertainty of ∼6%, and above that we have uncertainty of ∼20%. The phase uncertainties are small enough to have a negligible contribution to the possible amplitude uncertainty.

3.1. *Data selection*

As discussed in Section 2.1, for a few pulsars the electromagnetic observations did not always span the S6/VSR2,4 runs completely, and some pulsars glitched during the runs. As a result, we deal with these instances separately. In most cases, we can use all the data coherently, but, in other cases, sections of data must be combined incoherently. The relative sensitivities of the detectors at the pulsar frequencies also dictate whether we have used Virgo-only, LIGO-only or Virgo and LIGO data (see Fig. 1). For J0537−6910, only the LIGO data has been used because of its better sensitivity at the corresponding frequency, and results from each inter-glitch period have been combined incoherently. For J0835−4510 (the Vela pulsar), a glitch occurred just prior to VSR4 and we had no phase-connected timing solution between VSR2 (Abadie et al. 2011) and VSR4 epochs. The VSR2 results and VSR4 data have therefore been incoherently combined. For J1813−1246, the results from the pre- and post-glitch periods using all data from S6 and VSR2,4 have been combined incoherently. For J1833−1034, only VSR2 data up to the time of the observed glitch has been used.

The parameters and results (from the three different analyses discussed in Section 1.3) for the seven pulsars highlighted in Section 2.1 are given in Tables 4 and 5, respectively. Table 5 gives the 95% upper limit on the gravitational wave amplitude, $h_0^{95\%}$, the equivalent limits (via equation 3) on the stars fiducial ellipticity, ε, and mass quadrupole moment, Q_{22}, the ratio of the limit to the spin-down limit, $h_0^{95\%}/h_0^{\rm sd}$, and the limit on the gravitational wave luminosity compared to the total spin-down luminosity. This final value is given in the form of the percentage of the spin-down luminosity required to produce a gravitational wave at the amplitude limit (it can be seen from equation 4 that this is just the square of the ratio $h_0^{95\%}/h_0^{\rm sd}$). For those pulsars with constrained orientations (see Table 3) the results with and without the constraints are also given in Tables 5. Despite the very tight constraints given in Table 3 it should be noted that these results would only show minor differences if the angle (ι and ψ) errors were expanded to several times the given values. This is because the recovered posterior probability distributions on these parameters are slowly and smoothly varying over their parameter ranges. A brief discussion of the differences between the upper limits from the different methods is given in Section 1.3.

One of the new targets, J1824−2452I (which is an interesting pulsar that is seen to switch between being accretion and rotation powered Papitto et al. 2013), had a coherent timing solution that covered 2006, so S5 data from the LIGO detectors has been reanalyzed for this result. For all other pulsars, we have used only the VSR2 and VSR4 data if $f_{\rm gw} < 40$ Hz, and have coherently combined VSR2, VSR4 and S6 data from H1 and L1 for pulsars with $f_{\rm gw} > 40$ Hz. All the available science mode data (i.e., when the detectors were operating in a stable state) has been used, with details given in Table 1.

For the 19 pulsars with $f_{\rm gw} < 40$ Hz the results can be found in Table 7. Because of their low frequencies, none

[154] In Ng & Romani (2008) the inclination is denoted by ζ and the position angle Ψ is equivalent to our polarization angle. Our searches are insensitive to rotations of 90° in the polarization angle, so our quoted values are rotated into the range $-45° < \psi < 45°$.

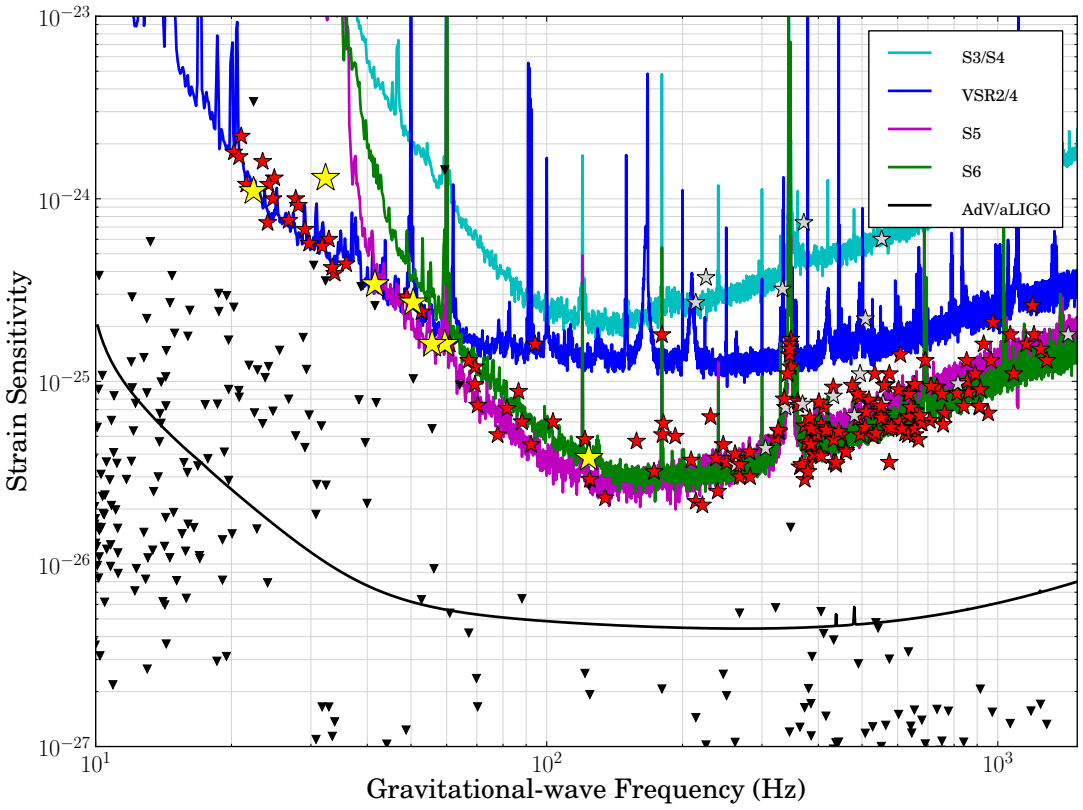

FIG. 1.— The $h_0^{95\%}$ upper limits (given by $\star$) for 195 pulsars from the LIGO and Virgo S3/S4, S5, S6, VSR2, and VSR4 runs. The curves give estimated relative strain sensitivities of these runs and potential future science runs. The sensitivities are based on the harmonic mean of the observation time (T) weighted one-sided power spectral densities S_n from all detectors operating during the given run, and are given by $10.8\sqrt{S_n/T}$, where the scale factor of 10.8 is given in Dupuis & Woan (2005). The AdV/aLIGO curve assumes a joint analysis of two equally sensitive advanced LIGO detectors and the advanced Virgo detector operating at their full design sensitivities with one year of coherent integration (the sensitivity curves are those given in Aasi et al. 2013c). The ▼ give the spin-down limits for all (non-Globular Cluster) pulsars, based on values taken from the ATNF catalog and assuming the canonical moment of inertia. The $\star$ show the observational upper limits from Tables 5, 7 and 8, with the seven high interest pulsars represented by the larger, lighter colored stars. Results for pulsars using the previous S3/S4 and S5 data are given by the small lighter colored stars.

TABLE 4
THE PROPERTIES OF THE PULSARS OF HIGH INTEREST.

Pulsar	α	δ	$f_{\rm rot}$ (Hz)	$f_{\rm gw}$ (Hz)	$\dot{f}_{\rm rot}$ (Hz/s)	d (kpc)	$\dot{E}^{\dagger}$ (W)	$h^{\rm sd\,\dagger}$
J0534+2200 (Crab)	$05^{\rm h}34^{\rm m}31\overset{\rm s}{.}97$	$22°00'52\overset{''}{.}07$	29.72	59.44	-3.7×10^{-10}	2.0[a]	4.6×10^{31}	1.4×10^{-24}
J0537−6910 (N157B)	$05^{\rm h}37^{\rm m}47\overset{\rm s}{.}36$	$-69°10'20\overset{''}{.}40$	61.97	123.94	-2.0×10^{-10}	50.0[b]	4.9×10^{31}	3.0×10^{-26}
J0835−4510 (Vela)	$08^{\rm h}35^{\rm m}20\overset{\rm s}{.}61$	$-45°10'34\overset{''}{.}88$	11.19	22.39	-1.6×10^{-11}	0.29[c]	6.9×10^{29}	3.3×10^{-24}
J1813−1246	$18^{\rm h}13^{\rm m}23\overset{\rm s}{.}74$	$-12°46'00\overset{''}{.}86$	20.80	41.60	-7.6×10^{-12}	1.9[d]	6.2×10^{29}	2.6×10^{-25}
J1833−1034 (G21.5−0.9)	$18^{\rm h}33^{\rm m}33\overset{\rm s}{.}61$	$-10°34'16\overset{''}{.}61$	16.16	32.33	-5.3×10^{-11}	4.8[e]	3.4×10^{30}	3.0×10^{-25}
J1913+1011	$19^{\rm h}13^{\rm m}20\overset{\rm s}{.}34$	$10°11'23\overset{''}{.}11$	27.85	55.70	-2.6×10^{-12}	4.5[f]	2.8×10^{29}	2.3×10^{-25}
J1952+3252 (CTB 80)	$19^{\rm h}52^{\rm m}58\overset{\rm s}{.}11$	$32°52'41\overset{''}{.}24$	25.30	50.59	-3.7×10^{-12}	3.0[f]	3.7×10^{29}	1.0×10^{-25}

† The spin-down luminosity, $\dot{E}$, and spin-down gravitational wave amplitude limit, $h^{\rm sd}$, both assume a canonical moment of inertia of $I_{zz} = 10^{38}\,{\rm kg\,m^2}$.
[a] See Appendix of Kaplan et al. (2008).
[b] Pietrzyński et al. (2013).
[c] Dodson et al. (2003).
[d] This distance is the average of the two estimates from Wang (2011), which allow a distance between ∼0.9–3.5 kpc.
[e] Tian & Leahy (2008).
[f] The distance is taken from the ATNF pulsar catalog (Manchester et al. 2005).

TABLE 5
Upper limits for the high interest pulsars. Limits with constrained orientations are given in parentheses.

Analysis	$h_0^{95\%}$	ε	Q_{22} (kg m^2)	$h_0^{95\%}/h_0^{\rm sd}$	$\dot{E}_{\rm gw}/\dot{E}$ %
			J0534+2200 (Crab)		
Bayesian	$1.6\,(1.4)\times10^{-25}$	$8.6\,(7.5)\times10^{-5}$	$6.6\,(5.8)\times10^{33}$	0.11 (0.10)	1.2 (1.0)
$\mathcal{F}/\mathcal{G}$-statistic	$2.3\,(1.8)\times10^{-25}$	$12.3\,(9.6)\times10^{-5}$	$11.6\,(7.4)\times10^{33}$	0.16 (0.13)	2.6 (1.7)
$5n$-vector	$1.8\,(1.6)\times10^{-25}$	$9.7\,(8.6)\times10^{-5}$	$7.4\,(6.6)\times10^{33}$	0.12 (0.11)	1.4 (1.2)
			J0537−6910		
Bayesian	$3.8\,(4.4)\times10^{-26}$	$1.2\,(1.4)\times10^{-4}$	$0.9\,(1.0)\times10^{34}$	1.4 (1.7)	200 (290)
$\mathcal{F}/\mathcal{G}$-statistic	$1.1\,(1.0)\times10^{-25}$	$3.4\,(3.1)\times10^{-4}$	$2.6\,(2.4)\times10^{34}$	4.1 (3.9)	1700 (1500)
$5n$-vector	$4.5\,(6.7)\times10^{-26}$	$1.4\,(2.1)\times10^{-4}$	$1.1\,(1.6)\times10^{34}$	1.6 (2.4)	260 (580)
			J0835−4510 (Vela)		
Bayesian	$1.1\,(1.0)\times10^{-24}$	$6.0\,(5.5)\times10^{-4}$	$4.7\,(4.2)\times10^{34}$	0.33 (0.30)	11 (9.0)
$\mathcal{F}/\mathcal{G}$-statistic	$4.2\,(9.0)\times10^{-25}$	$2.3\,(4.9)\times10^{-4}$	$1.8\,(3.8)\times10^{34}$	0.13 (0.27)	1.7 (7.3)
$5n$-vector	$1.1\,(1.1)\times10^{-24}$	$6.0\,(6.0)\times10^{-4}$	$4.7\,(4.7)\times10^{34}$	0.33 (0.33)	11 (11)
			J1813−1246		
Bayesian	3.4×10^{-25}	3.5×10^{-4}	2.7×10^{34}	1.3	170
$\mathcal{F}/\mathcal{G}$-statistic	7.1×10^{-25}	7.4×10^{-4}	5.7×10^{34}	2.7	730
$5n$-vector	4.8×10^{-25}	4.9×10^{-4}	3.8×10^{34}	1.8	320
			J1833−1034		
Bayesian	$1.3\,(1.4)\times10^{-24}$	$5.7\,(6.1)\times10^{-3}$	$4.4\,(4.7)\times10^{35}$	4.3 (4.6)	1800 (2100)
$\mathcal{F}/\mathcal{G}$-statistic	$1.2\,(1.2)\times10^{-24}$	$5.2\,(5.2)\times10^{-3}$	$4.0\,(4.0)\times10^{35}$	3.9 (3.9)	1500 (1500)
$5n$-vector	$1.4\,(2.0)\times10^{-24}$	$6.1\,(8.7)\times10^{-3}$	$4.7\,(6.7)\times10^{35}$	4.6 (6.6)	2100 (4400)
			J1913+1011		
Bayesian	1.6×10^{-25}	2.2×10^{-4}	1.7×10^{34}	2.9	840
$\mathcal{F}/\mathcal{G}$-statistic	2.9×10^{-25}	4.1×10^{-4}	3.1×10^{34}	5.3	2800
$5n$-vector	2.5×10^{-25}	3.4×10^{-4}	2.7×10^{34}	4.5	2000
			J1952+3252		
Bayesian	$2.7\,(2.5)\times10^{-25}$	$3.0\,(2.8)\times10^{-4}$	$2.3\,(2.1)\times10^{34}$	2.6 (2.5)	680 (630)
$\mathcal{F}/\mathcal{G}$-statistic	6.0×10^{-25}	6.7×10^{-4}	5.1×10^{34}	5.8	3400
$5n$-vector	$3.1\,(3.2)\times10^{-25}$	$3.4\,(3.5)\times10^{-4}$	$2.6\,(2.7)\times10^{34}$	3.0 (3.1)	900 (960)

Note. — Detector calibration errors mean that for pulsars with $f_{\rm gw}$ below and above 50 Hz (see Table 4) there are ∼6% and ∼20% uncertainties respectively on these limits.

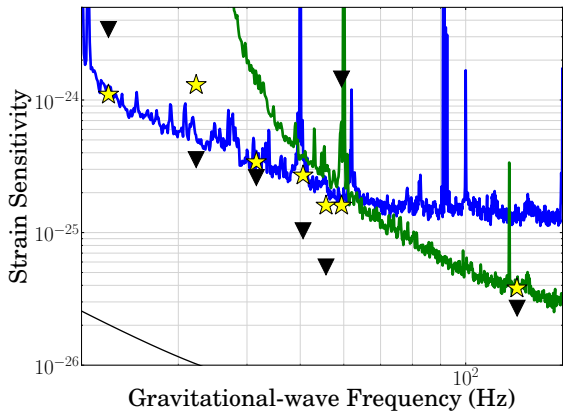

FIG. 2.— A zoomed version of Figure 1 focusing on the seven high interest pulsars. The outlier at ∼32 Hz is J1833−1034 for which only VSR2 data was used.

of these pulsars had been targeted before.

Results for pulsars with $f_{\rm gw} > 40\,$Hz using S6 and VSR2,4 are shown in Table 8. Distances to pulsars in Terzan 5 (with designations J1748−2446) are assumed to be 5.5 kpc (Ortolani et al. 2007) rather than the value of 8.7 kpc given in the ATNF catalog, and distances to the pulsars in M28 (with designations J1824−2452) are assumed to be 5.5 kpc (Harris 1996) rather than the distance of 4.9 kpc given in Abbott et al. (2010). Unless otherwise specified in the table for all other pulsars we use the distance values given by the `DIST` value in the ATNF catalog (Manchester et al. 2005), which generally are dispersion measure calculations from the electron density distribution model of Taylor & Cordes (1993). For the 16 pulsars where new timing solutions were not available during the most recent runs (see Section 2.1), we include the results from the LIGO S3/S4 (Abbott et al. 2007b) and S5 analysis (Abbott et al. 2010).

The gravitational wave amplitude upper limits as a function of frequency are plotted in Fig. 1 and Fig. 2 (showing a version just containing the seven high interest pulsars), which also show bands giving the expected sensitivity of the analysis. The upper limits in histogram form for all pulsars can be seen in Fig. 3. The histograms show that the distribution of h_0 upper limits is peaked just below 10^{-25}, corresponding to equivalent peaks on ε and Q_{22} of $\sim 10^{-6}$ and $\sim 10^{-32}\,\mathrm{kg\,m^2}$. The spin-down limit ratios shows that we are within a factor of 100 for just over half of the pulsars. It is interesting to see that due to the shape of the detector sensitivity curves the lower frequency young pulsars (analysed only with Virgo data) have the highest amplitude limits, but as several have high spin-down luminosities they have an approximately uniform spread in spin-down limit ratios.

4. DISCUSSION

We have seen no credible evidence for gravitational wave emission from any known pulsar, but have been able to place upper limits on the gravitational wave amplitude from an unprecedented number of pulsars. In this work we have produced entirely new results for 73 pulsars and updated the results of previously searches for 106 pulsars, with results from a further 16 from previous analyses being reproduced here. A total of 195 pulsars have now been targeted over the lifetimes of the first generation of interferometric gravitational wave detectors.

4.1. *Quadrupole estimates*

As discussed in the introduction, we have targeted the gravitational-wave signature of the time-varying $l = m = 2$ quadrupole moment. There is great uncertainty, however, as to whether neutron stars can form and sustain sufficient elastic deformations to give an observable quadrupole, and this, in turn, makes it difficult to model a realistic source population. The recent work by Johnson-McDaniel & Owen (2013) (also see e.g. Owen 2005; Pitkin 2011) on the maximum sustainable quadrupole for a variety of neutron star equations of state indicates that relatively large quadrupoles can indeed be sustained. Johnson-McDaniel & Owen (2013) find that solid quark stars could sustain quadrupoles of up to $10^{37}\,\mathrm{kg\,m^2}$ (or fiducial ellipticities of order 0.1), hybrid stars could sustain quadrupoles of up to $10^{35}\,\mathrm{kg\,m^2}$ (or fiducial ellipticities of order 1×10^{-3}), while for normal neutron stars the stiffest equations of state allow quadrupoles of $\sim 1\times10^{33}\,\mathrm{kg\,m^2}$ (or fiducial ellipticities of $\sim 1\times10^{-5}$). It is worth noting that these are maximum allowable quadrupoles, and it is still unknown whether they are realized in nature for reasons described in Abbott et al. (2007a).

A mass quadrupole may also be generated by distortional pressure from the star's magnetic field (see e.g. Bonazzola & Gourgoulhon 1996; Cutler 2002; Ciolfi et al. 2010). The external dipole field of a pulsar is usually estimated from its rotational spin-down, assuming this is due to magnetic dipole radiation (equivalent to the gravitational wave spin-down limit that we define). As discussed in Section 2, this gives external surface dipole field strengths of $\sim 10^9\,$G for MSPs and $\sim 10^{12}\,$G for normal pulsars. Internal fields of this magnitude are too small to induce mass quadrupoles that would be currently observable, but the field strengths of some magnetars are at a suitable level (though rotating too slowly to be detectable sources for ground-based gravitational wave detectors). Unfortunately, internal field strengths and configurations are not well understood, and the mechanisms for burying fields beneath the surface are uncertain. Studies of one young pulsar with a braking index of $n \approx 1$ (Espinoza et al. 2011) may point towards an evolving and increasing external magnetic field, with an internal field leaking out over time, but recently other mechanisms have been proposed to explain the evolution of the field that do not rely on an increasing magnetic field (e.g. Ho & Andersson 2012; Çalişkan et al. 2013). Mastrano & Melatos (2012) discuss the prospects of constraining field strength and configuration for recycled MSPs using gravitational wave data. This is also discussed in Pitkin (2011), who shows limits that could be obtained on fully poloidal or toroidal field configurations. Further estimates of the quadrupoles that can be generated by internal magnetic fields for a given equation of state are given in Haskell et al. (2008, 2009); Akgun & Wasserman (2007).

4.2. *High interest pulsars*

For the seven high interest pulsars the results are all close to (or beat) the spin-down limits. In particular, our upper limits are significantly below the spin-down

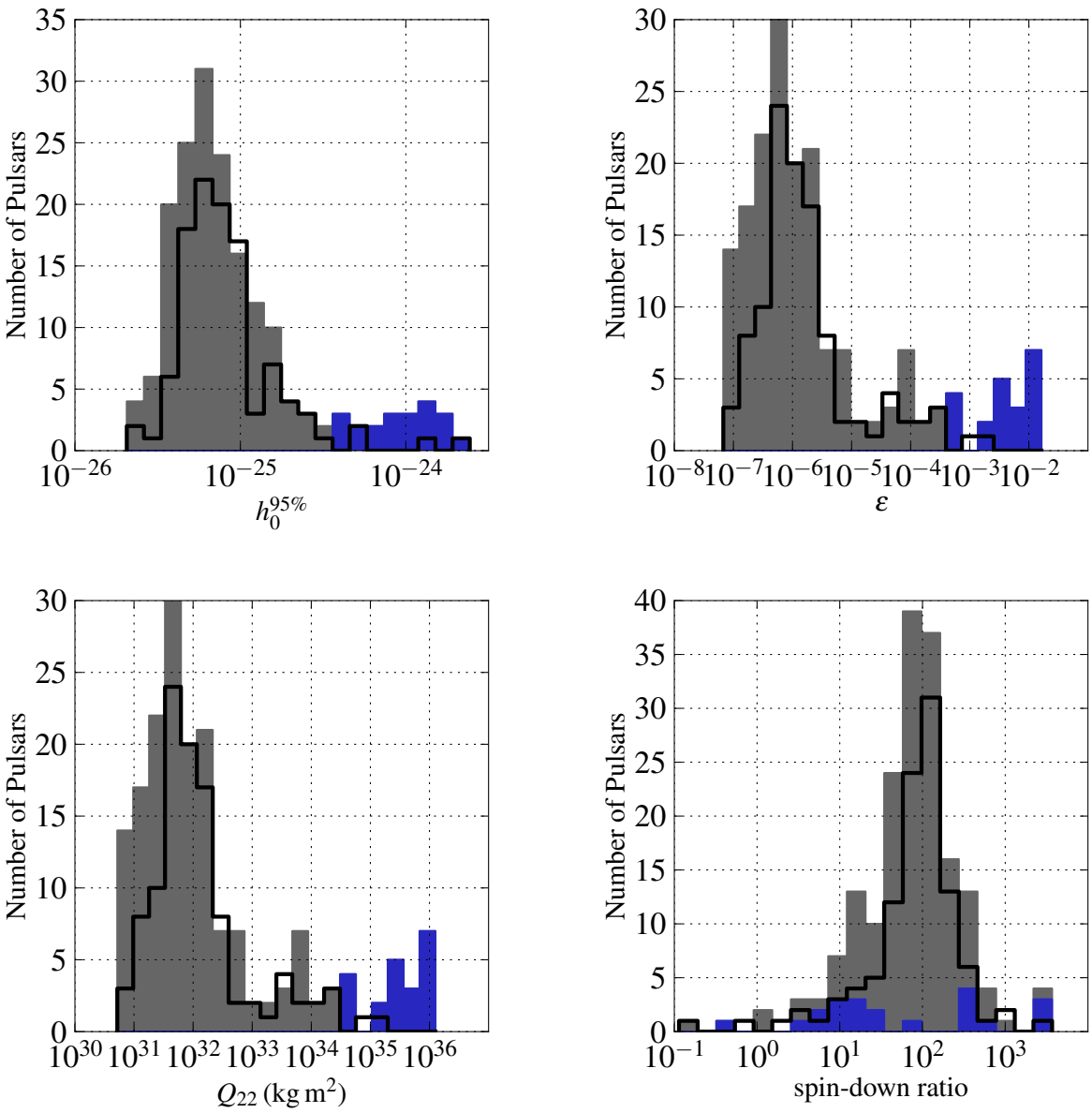

FIG. 3.— The upper limits in histogram form for all pulsars for h_0, ε, Q_{22} and the spin-down limit ratio. The grey shaded area represents results from the S6/VSR2,4 analysis combining all detectors, the blue shaded area represents results from the VSR2,4-only analyses. These also contain the seven high interest pulsars for which the Bayesian method values have been plotted based on no assumptions about the pulsar orientations. Previous upper limits from the S5 analysis are given by the unfilled histogram.

limit for the Crab and Vela pulsars, further improving over past results. The mass quadrupole limits are generally within 10^{34}–$10^{35}\,\mathrm{kg\,m^2}$, with the Crab pulsar upper limit slightly lower at $\sim 7\times10^{33}\,\mathrm{kg\,m^2}$. Therefore, for these stars to emit gravitational waves at current sensitivities the emission would most likely have to come from a quark star or one with a hybrid core, whilst the Crab pulsar is about an order of magnitude above the maximum quadrupoles expected for purely crustal emission. However, for advanced detectors the sensitivity for Crab pulsar would be consistent with most optimistic predictions for *normal* neutron stars. For J0537−6910, which has a quadrupole limit close to the Crab pulsar, future prospects may not be so good for reaching the most optimistic prediction for *normal* neutron stars. This is due to the requirement for phase coherent timing, which for these analyses relied on the no-longer-operational RXTE.

For the Crab and Vela pulsars, our results now limit the gravitational wave emission to contribute $\lesssim 1\%$ and $\lesssim 10\%$ of their respective spin-down luminosities, with an improvement of about a factor of 4 for Vela with respect to previous results. These limits are compatible with the observed braking indices of the pulsars, which are $n = 2.51$ and $n \approx 1.4$ respectively (see e.g. Palomba 2000).

Given various assumptions about the magnetic field discussed above, our results constrain the internal field of the Crab pulsar to be less than $\sim 10^{16}$ G (e.g. Cutler 2002). For the other high interest pulsars, the limits on the magnetic field would be even higher than this, so we

have not included them here.

Johnson-McDaniel (2013) relates the limits on the $l = m = 2$ quadrupole moment from the gravitational wave emission to the physical surface deformation of a star for a variety of equations of state, which can be compared to the oblateness due to rotation (note that there is no particular reason to expect a relation between these quantities). His results showed that previous gravitational wave limits for the Crab pulsar constrained the surface deformation from the $l = m = 2$ quadrupole to be well below the rotational deformation for all equations of state and neutron star masses. Our new results slightly improve these limits, with the physical surface deformation limited to less than $\sim$30 cm, maximized over masses and equations of state. For the Vela pulsar, our new results limit non-axisymmetric quadrupole deformations to be $\lesssim 100$ cm, which is smaller than the expected rotational oblateness for equations of state with large radii.

For PSR J0537−6910, the quality of S6 data at the corresponding frequency was relatively poor, and the upper limits are no better than those produced during S5 (Abbott et al. 2010). If this pulsar were, however, at the upper end of the moment of inertia range ($\sim 3\times10^{38}\,\mathrm{kg\,m^2}$) the spin-down limit would be increased by a factor of $\sim$1.7, and we would now fall below it[155].

4.3. *Other highlights*

Several other pulsar upper limits are within a factor of 10 of their spin-down limits. For the MSPs, three upper limits are within a factor of ten of the spin-down limit: J1045−4509, a factor of 6; J1643−1224, a factor of 10; and J2124−3358, also a factor of 10. The upper limit that corresponds to the smallest ellipticity/mass quadrupole is from J2124−3358 with $\varepsilon = 6.7\times10^{-8}$ and $Q_{22} = 5.2\times10^{30}\,\mathrm{kg\,m^2}$. Although this value is currently above the spin-down limit, it is well within allowable maximum deformations for all neutron star equations of state (see e.g. Pitkin 2011). The gravitational wave spin-down limits for these pulsars require quadrupoles that are well within reasonable theoretical ranges, so they will make intriguing targets for the advanced generation of detectors.

For the young pulsars only targeted with Virgo VSR2 and VSR4 data a further five are within a factor of ten of the spin-down limit (see Table 7). All of these would be required to have an exotic equation of state to be observed at around their spin-down limits in future detectors.

4.4. *Future prospects*

The search results described in this paper assume that the pulsar gravitational-wave phase evolution is very well known and tied very closely to the observed electromagnetic phase. However, precession (e.g. Zimmermann & Szedenits 1979; Jones & Andersson 2002) or other models (Jones 2010) could give emission at both the rotation frequency and twice the rotation frequency. Additionally, as discussed in Abbott et al. (2008), emission may be offset from the electromagnetic phase model. We therefore will be applying methods to search for gravitational waves from known pulsars at multiple harmonics and with narrow bandwidths around the observed electromagnetic values in archival and future datasets.

We look forward to the era of the *advanced* LIGO (aLIGO) (Harry & LIGO Scientific Collaboration 2010) and Virgo (AdV) (Acernese et al. 2009; Accadia et al. 2012) detectors (see Aasi et al. 2013c, for estimates of the aLIGO and AdV observation schedule and sensitivity evolution), as well as the KAGRA detector (Somiya 2012). Ongoing radio pulsar surveys are discovering new objects that will be targeted with future detectors. Currently, the High Time Resolution Universe survey with the Parkes and Effelsberg telescopes (Keith et al. 2010) has discovered 29 new MSPs (Keith 2013; Ng et al. 2013) and could discover up to $\sim$75 once complete. The high sensitivity Arecibo PALFA survey is discovering new pulsars (Lazarus 2013) and making use of distributed computing through Einstein@home (Allen et al. 2013). The Green Bank Drift-scan survey and the Green Bank North Celestial Cap survey are also discovering new and interesting sources (Lynch et al. 2013). Many interesting high energy pulsars, undetectable in the radio frequency band, are also being detected by the *Fermi* Large Area Telescope (Saz Parkinson et al. 2013). *Fermi* is also providing targets to facilitate radio searches which are finding many new MSPs. In addition, new analyses of archive data, such as using Einstein@home to search through Parkes Multi-beam Pulsar Survey data, are still yielding new results (Knispel et al. 2013). In the near future, there are exciting prospects from the Low Frequency Array (LOFAR), which could detect the majority of radio pulsars within $\sim$2 kpc, giving of order 1000 new pulsars (van Leeuwen & Stappers 2010; Stappers et al. 2011), and perform deep searches for pulsars in globular clusters.

Finally, we should emphasize that known pulsar searches are not the only searches looking for gravitational waves from rotating, galactic neutron stars. There have been, or are under way, several directed searches looking for sources of unknown frequency and spin-down in particular objects e.g. globular clusters, supernova remnants (e.g. Abadie et al. 2010; Chung et al. 2011), the Galactic center (Aasi et al. 2013a), and low-mass X-ray binaries. There are also several semi-coherent, all-sky, wide-frequency band searches (e.g. Abadie et al. 2012; Aasi et al. 2013b). Very similar pipelines will be used during the advanced detector era, yielding signal candidates, performing follow-ups and, in case of detection, source parameter estimation.

The authors gratefully acknowledge the support of the United States National Science Foundation for the construction and operation of the LIGO Laboratory, the Science and Technology Facilities Council of the United Kingdom, the Max-Planck-Society, and the State of Niedersachsen/Germany for support of the construction and operation of the GEO600 detector, and the Italian Istituto Nazionale di Fisica Nucleare and the French Centre National de la Recherche Scientifique for the construction and operation of the Virgo detector. The authors also gratefully acknowledge the support of the research by these agencies and by the Australian Re-

[155] The distance to the Large Magellanic Cloud is known to $\sim$2% (Pietrzyński et al. 2013), so does not significantly contribute to the uncertainty on the spin-down limit.

TABLE 6
RXTE ephemerides for J0537−6910 during the period of S6, VSR2, and VSR4.

EM Observation Span (MJD and date)	Epoch t_0 ($\mathrm{MJD_{TDB}}$)	$f_{\rm rot}$ (Hz)	$\dot{f}_{\rm rot}$ (10^{-10} Hz/s)	$\ddot{f}_{\rm rot}$ (10^{-20} Hz/s^2)
54897 (2009 Mar 7) – 55041 (2009 Jul 29)	54966.4266616022	61.9765822442	−1.9948300	0.960
55045 (2009 Aug 2) – 55182 (2009 Dec 17)	55140.0377727133	61.9736036203	−1.9939924	2.090
55185 (2009 Dec 20) – 55263 (2010 Mar 8)	55221.0562912318	61.9722204755	−1.9951973	2.090
55275 (2010 Mar 20) – 55445 (2010 Sep 6)	55313.6488838244	61.9706584446	−1.9953330	0.673
55458 (2010 Sep 19) – 55503 (2010 Nov 3)	55475.6859208615	61.9678758925	−1.9952574	0.673

search Council, the International Science Linkages program of the Commonwealth of Australia, the Council of Scientific and Industrial Research of India, the Istituto Nazionale di Fisica Nucleare of Italy, the Spanish Ministerio de Economía y Competitividad, the Conselleria d'Economia Hisenda i Innovació of the Govern de les Illes Balears, the Foundation for Fundamental Research on Matter supported by the Netherlands Organisation for Scientific Research, the Polish Ministry of Science and Higher Education, the FOCUS Programme of Foundation for Polish Science, the Royal Society, the Scottish Funding Council, the Scottish Universities Physics Alliance, the National Aeronautics and Space Administration, OTKA of Hungary, the Lyon Institute of Origins (LIO), the National Research Foundation of Korea, Industry Canada and the Province of Ontario through the Ministry of Economic Development and Innovation, the National Science and Engineering Research Council Canada, the Carnegie Trust, the Leverhulme Trust, the David and Lucile Packard Foundation, the Research Corporation, and the Alfred P. Sloan Foundation. The Nançay Radio Observatory is operated by the Paris Observatory, associated with the French Centre National de la Recherche Scientifique. LIGO Document No. LIGO-P1200104.

APPENDIX

EPHEMERIS FOR J0537−6910

Over the span of S6, VSR2, and VSR4 RXTE made observations of J0537−6910. It was observed to glitch four times during this period and phase connected ephemerides were produced for each inter-glitch segment. These ephemerides, given in Table 6, use a DE200 sky position of $\alpha = 05^{\rm h}37^{\rm m}47\overset{\rm s}{.}36$ and $\delta = -69°10'20\overset{''}{.}4$ (Wang et al. 2001).

REFERENCES

Aasi, J. et al. 2012, Class. Quant. Grav. 29, 155002
—. 2013a, arXiv:1309.6221
—. 2013b, Phys. Rev. D, 87, 042001
—. 2013c, arXiv:1304.0670
Abadie, J. et al. 2010, ApJ, 722, 1504
—. 2011, ApJ, 737, 93
—. 2012, Phys. Rev. D, 85, 022001
Abbott, B. et al. 2004, Phys. Rev. D, 69, 082004
—. 2005, Phys. Rev. Lett., 94, 181103
—. 2007a, Phys. Rev. D, 76, 082001
—. 2007b, Phys. Rev. D, 76, 042001
—. 2008, ApJ, 683, L45
Abbott, B. P. et al. 2009, Rep. Prog. Phys., 72, 076901
—. 2010, ApJ, 713, 671
Abdo, A. A. et al. 2009, Science, 325, 840
Accadia, T. et al. 2011, Class. Quant. Grav. 28, 025005
—. 2012, Advanced Virgo Technical Design Report, Tech. Rep. VIR-0128A-12, https://tds.ego-gw.it/ql/?c=8940
Acernese, F. et al. 2009, Advanced Virgo Baseline Design, Tech. Rep. VIR-0027A-09, https://tds.ego-gw.it/ql/?c=6589
Adhikari, R., Fritschel, P., & Waldman, S. 2006, Enhanced LIGO, Tech. Rep. LIGO-T060156-v01, California Institute of Technology, Massachusetts Institute of Technology, https://dcc.ligo.org/LIGO-T060156-v1/public
Akgun, T. & Wasserman, I. 2007, MNRAS, 383, 1551
Allen, B. et al. 2013, ApJ, 773, 91
Astone, P., Colla, A., D'Antonio, S., Frasca, S., & Palomba, C. 2012, Journal of Physics Conference Series, 363, 012038
Astone, P., D'Antonio, S., Frasca, S., & Palomba, C. 2010, Class. Quant. Grav. 27, 194016
Bartos, I. et al. 2011, Frequency Domain Calibration Error Budget for LIGO in S6, Tech. Rep. LIGO-T1100071-v9, LIGO Laboratory, https://dcc.ligo.org/LIGO-T1100071-v9/public
Bonazzola, S. & Gourgoulhon, E. 1996, A&A, 312, 675
Brooks, S. P. & Roberts, G. O. 1998, Statistics and Computing, 8, 319
Buchner, S. 2010, The Astronomer's Telegram, 2768
Çalişkan, Ş., Ertan, Ü., Alpar, M. A., Trümper, J. E., & Kylafis, N. D. 2013, MNRAS
Chung, C. T. Y., Melatos, A., Krishnan, B., & Whelan, J. T. 2011, MNRAS, 414, 2650
Ciolfi, R., Ferrari, E., & Gualtieri, L. 2010, MNRAS, 406, 2540
Cordes, J. M. & Lazio, T. J. W. 2002, arXiv:astro-ph/0207156
Cutler, C. 2002, Phys. Rev. D, 66, 084025
Dodson, R., Legge, D., Reynolds, J. E., & McCulloch, P. M. 2003, ApJ, 596, 1137
Dupuis, R. J. & Woan, G. 2005, Phys. Rev. D, 72, 102002
Espinoza, C. M., Lyne, A. G., Kramer, M., Manchester, R. N., & Kaspi, V. M. 2011, ApJ, 741, L13
Feldman, G. J. & Cousins, R. D. 1998, Phys. Rev. D, 57, 3873
Ferrari, A. & Ruffini, R. 1969, ApJ, 158, L71
Harris, W. E. 1996, AJ, 112, 1487
Harry, G. M. & LIGO Scientific Collaboration. 2010, Class. Quant. Grav. 27, 084006
Haskell, B., Samuelsson, L., Glampedakis, K., & Andersson, N. 2008, MNRAS, 385, 531
—. 2009, MNRAS, 394, 1711
Helfand, D. J., Taylor, J. H., Backus, P. R., & Cordes, J. M. 1980, ApJ, 237, 206
Ho, W. C. G. & Andersson, N. 2012, Nature Physics, 8, 787
Hobbs, G. B., Edwards, R. T., & Manchester, R. N. 2006, MNRAS, 369, 655
Jaranowski, P. & Królak, A. 2010, Class. Quant. Grav. 27, 194015
Johnson-McDaniel, N. K. 2013, Phys. Rev. D, 88, 044016
Johnson-McDaniel, N. K. & Owen, B. J. 2013, Phys. Rev. D, 88, 044004
Jones, D. I. 2010, MNRAS, 402, 2503
Jones, D. I. & Andersson, N. 2002, MNRAS, 331, 203
Kaplan, D. L., Chatterjee, S., Gaensler, B. M., & Anderson, J. 2008, ApJ, 677, 1201
Keith, M. J. 2013, in IAU Symposium, Vol. 291, IAU Symposium, 29–34

TABLE 7
LIMITS ON THE GRAVITATIONAL WAVE AMPLITUDE FOR KNOWN PULSARS WITH $f_{\rm gw} < 40\,$Hz USING VSR2,4 DATA

Pulsar	$f_{\rm rot}$ (Hz)	$f_{\rm gw}$ (Hz)	$\dot{f}_{\rm rot}$ (Hz/s)	d (kpc)	$h_0^{\rm sd}$	$h_0^{95\%}$	ε	Q_{22} (kg m^2)	$h_0^{95\%}/h_0^{\rm sd}$
J0106+4855	12.03	24.05	-6.2×10^{-14}	7.3	7.9×10^{-27}	7.4×10^{-25}	8.9×10^{-3}	6.9×10^{35}	94
J0609+2130	17.95	35.91	-7.6×10^{-17}	1.8	9.1×10^{-28}	4.4×10^{-25}	5.9×10^{-4}	4.6×10^{34}	490
J1528−3146	16.44	32.88	-6.7×10^{-17}	1.0	1.6×10^{-27}	6.0×10^{-25}	5.2×10^{-4}	4.0×10^{34}	360
J1718−3825	13.39	26.78	-2.4×10^{-12}	4.2	8.0×10^{-26}	7.6×10^{-25}	4.2×10^{-3}	3.3×10^{35}	9.5
J1747−2958	10.12	20.24	-6.3×10^{-12}	2.5	2.6×10^{-25}	1.8×10^{-24}	1.0×10^{-2}	7.9×10^{35}	7.0
J1748−2446J	12.45	24.89	-2.0×10^{-16}	5.5	5.8×10^{-28}‡	1.3×10^{-24}	1.1×10^{-2}	8.3×10^{35}	2200
J1753−1914	15.88	31.77	-4.9×10^{-16}	2.8	1.6×10^{-27}	5.5×10^{-25}	1.4×10^{-3}	1.1×10^{35}	340
J1753−2240	10.51	21.02	-6.9×10^{-17}	3.5	6.0×10^{-28}	2.2×10^{-24}	1.6×10^{-2}	1.3×10^{36}	3700
J1809−1917	12.08	24.17	-3.7×10^{-12}	3.7	1.2×10^{-25}	1.2×10^{-24}	7.2×10^{-3}	5.6×10^{35}	9.9
J1828−1101	13.88	27.76	-2.9×10^{-12}	7.3	5.0×10^{-26}	1.0×10^{-24}	9.2×10^{-3}	7.1×10^{35}	20
J1831−0952	14.87	29.73	-1.8×10^{-12}	4.3	6.5×10^{-26}	5.7×10^{-25}	2.6×10^{-3}	2.0×10^{35}	8.7
J1833−0827	11.72	23.45	-1.3×10^{-12}	4.5	5.9×10^{-26}†	1.6×10^{-24}	1.2×10^{-2}	9.6×10^{35}	27
J1856+0245	12.36	24.72	-9.5×10^{-12}	10.3	6.9×10^{-26}	10.0×10^{-25}	1.6×10^{-2}	1.2×10^{36}	15
J1904+0412	14.07	28.13	-2.8×10^{-17}	4.0	2.8×10^{-28}	9.2×10^{-25}	4.4×10^{-3}	3.4×10^{35}	3300
J1915+1606	16.94	33.88	-2.5×10^{-15}	7.1	1.4×10^{-27}†	3.9×10^{-25}	2.3×10^{-3}	1.7×10^{35}	280
J1928+1746	14.55	29.10	-2.8×10^{-12}	8.1	4.3×10^{-26}	6.8×10^{-25}	6.2×10^{-3}	4.8×10^{35}	16
J1954+2836	10.79	21.57	-2.5×10^{-12}	1.6	2.4×10^{-25}	1.2×10^{-24}	4.0×10^{-3}	3.1×10^{35}	5.1
J2043+2740	10.40	20.80	-1.3×10^{-13}	1.1	8.1×10^{-26}	1.7×10^{-24}	4.1×10^{-3}	3.2×10^{35}	21
J2235+1506	16.73	33.46	-2.9×10^{-17}	1.1	9.2×10^{-28}†	4.2×10^{-25}	4.0×10^{-4}	3.1×10^{34}	450

NOTE. — Detector calibration errors mean that for these pulsars there are ∼6% uncertainties on these limits.

† The pulsar's spin-down is corrected for proper motion effects.
‡ The pulsar's spin-down is calculated using a characteristic spin-down age of 10^9 years.

Keith, M. J., Jameson, A., van Straten, W., Bailes, M., Johnston, S., Kramer, M., Possenti, A., Bates, S. D., Bhat, N. D. R., Burgay, M., Burke-Spolaor, S., D'Amico, N., Levin, L., McMahon, P. L., Milia, S., & Stappers, B. W. 2010, MNRAS, 409, 619
Knispel, B. & Allen, B. 2008, Phys. Rev. D, 78, 044031
Knispel, B. et al. 2013, ApJ, 774, 93
Lazarus, P. 2013, in IAU Symposium, Vol. 291, IAU Symposium, 35–40
Lorimer, D. R. 2008, Living Reviews in Relativity, 11, 8
Lynch, R. S. et al. 2013, in IAU Symposium, Vol. 291, IAU Symposium, 41–46
Lyne, A. G., Pritchard, R. S., & Graham-Smith, F. 1993, MNRAS, 265, 1003, http://www.jb.man.ac.uk/research/pulsar/crab.html
Manchester, R. N., Hobbs, G. B., Teoh, A., & Hobbs, M. 2005, AJ, 129, 1993
Marshall, F. E., Gotthelf, E. V., Zhang, W., Middleditch, J., & Wang, Q. D. 1998, ApJ, 499, L179
Mastrano, A. & Melatos, A. 2012, MNRAS, 421, 760
Melosh, H. J. 1969, Nature, 224, 781
Middleditch, J., Marshall, F. E., Wang, Q. D., Gotthelf, E. V., & Zhang, W. 2006, ApJ, 652, 1531
Mours, B. & Rolland, L. 2011, h(t) reconstruction for VSR4, Tech. Rep. VIR-0704A-11, https://tds.ego-gw.it/ql/?c=8762
Ng, C. et al. 2013, in IAU Symposium, Vol. 291, IAU Symposium, 53–56
Ng, C.-Y. & Romani, R. W. 2004, ApJ, 601, 479
—. 2008, ApJ, 673, 411
Ortolani, S., Barbuy, B., Bica, E., Zoccali, M., & Renzini, A. 2007, A&A, 470, 1043
Ostriker, J. P. & Gunn, J. E. 1969, ApJ, 157, 1395
Owen, B. J. 2005, Phys. Rev. Lett., 95, 211101
—. 2006, Class. Quant. Grav. 23, 1
Palomba, C. 2000, A&A, 354, 163
—. 2005, MNRAS, 359, 1150
Papitto, A. et al. 2013, arXiv:1305.3884
Pietrzyński, G. et al. 2013, Nature, 495, 76
Pitkin, M. 2011, MNRAS, 415, 1849
Ray, P. S. et al. 2011, ApJS, 194, 17
Röver, C., Messenger, C., & Prix, R. 2011, arXiv:1103.2987
Roy, J., Gupta, Y., & Lewandowski, W. 2012, MNRAS, 424, 2213
Saz Parkinson, P. M. et al. 2013, in IAU Symposium, Vol. 291, IAU Symposium, 81–86
Shklovskii, I. S. 1969, AZh, 46, 715
Somiya, K. 2012, Class. Quant. Grav. 29, 124007
Stappers, B. W. et al. 2011, A&A, 530, A80
Taylor, J. H. & Cordes, J. M. 1993, ApJ, 411, 674
Tian, W. W. & Leahy, D. A. 2008, MNRAS, 391, L54
Ushomirsky, G., Cutler, C., & Bildsten, L. 2000, MNRAS, 319, 902
van Leeuwen, J. & Stappers, B. W. 2010, A&A, 509, A7
Wang, Q. D., Gotthelf, E. V., Chu, Y.-H., & Dickel, J. R. 2001, ApJ, 559, 275
Wang, W. 2011, Research in Astronomy and Astrophysics, 11, 824
Zimmermann, M. & Szedenits, Jr., E. 1979, Phys. Rev. D, 20, 351

TABLE 8
LIMITS ON THE GRAVITATIONAL WAVE AMPLITUDE FOR KNOWN PULSARS WITH $f_{\rm gw} > 40\,{\rm Hz}$

Pulsar	$f_{\rm rot}$ (Hz)	$f_{\rm gw}$ (Hz)	$\dot{f}_{\rm rot}$ (Hz/s)	d (kpc)	$h_0^{\rm sd}$	prior $h_0^{95\%}$	S6/VSR2,4 $h_0^{95\%}$	ε	Q_{22} (kg m^2)	$h_0^{95\%}/h_0^{\rm sd}$
J0023+0923	327.85	655.69	-1.3×10^{-15}	0.9	1.7×10^{-27}	...	6.9×10^{-26}	1.5×10^{-7}	1.1×10^{31}	41
J0024−7204C	173.71	347.42	1.6×10^{-15}	4.0	6.1×10^{-28}†	5.8×10^{-25}	1.7×10^{-25}	5.5×10^{-6}	4.2×10^{32}	290
J0024−7204D	186.65	373.30	1.6×10^{-16}	4.0	1.8×10^{-28}†	4.5×10^{-26}	2.9×10^{-26}	7.8×10^{-7}	6.1×10^{31}	160
J0024−7204E	282.78	565.56	-7.8×10^{-15}	4.0	1.1×10^{-27}†	9.9×10^{-26}	9.7×10^{-26}	1.1×10^{-6}	8.9×10^{31}	92
J0024−7204F	381.16	762.32	-9.3×10^{-15}	4.0	9.9×10^{-28}†	8.8×10^{-26}	6.7×10^{-26}	4.4×10^{-7}	3.4×10^{31}	67
J0024−7204G	247.50	495.00	2.6×10^{-15}	4.0	6.6×10^{-28}†	9.9×10^{-26}	8.2×10^{-26}	1.3×10^{-6}	9.8×10^{31}	120
J0024−7204H	311.49	622.99	3.0×10^{-16}	4.0	2.0×10^{-28}†	6.5×10^{-26}	5.2×10^{-26}	5.1×10^{-7}	3.9×10^{31}	260
J0024−7204I	286.94	573.89	3.9×10^{-15}	4.0	7.4×10^{-28}†	5.2×10^{-26}	5.8×10^{-26}	6.7×10^{-7}	5.2×10^{31}	79
J0024−7204J	476.05	952.09	2.4×10^{-15}	4.0	4.5×10^{-28}†	1.0×10^{-25}	6.6×10^{-26}	2.8×10^{-7}	2.1×10^{31}	150
J0024−7204L	230.09	460.18	-3.6×10^{-15}	4.0	8.0×10^{-28}‡	5.8×10^{-26}	4.2×10^{-26}	7.4×10^{-7}	5.7×10^{31}	52
J0024−7204M	271.99	543.97	-4.3×10^{-15}	4.0	8.0×10^{-28}‡	6.2×10^{-26}	7.0×10^{-26}	9.0×10^{-7}	7.0×10^{31}	88
J0024−7204N	327.44	654.89	2.5×10^{-15}	4.0	5.6×10^{-28}†	8.4×10^{-26}	5.1×10^{-26}	4.5×10^{-7}	3.5×10^{31}	91
J0024−7204O	378.31	756.62	-4.2×10^{-15}	4.0	6.7×10^{-28}†	9.3×10^{-26}	5.8×10^{-26}	3.8×10^{-7}	3.0×10^{31}	86
J0024−7204Q	247.94	495.89	-3.9×10^{-15}	4.0	8.0×10^{-28}‡	5.8×10^{-26}	5.1×10^{-26}	7.9×10^{-7}	6.1×10^{31}	64
J0024−7204R	287.32	574.64	-4.6×10^{-15}	4.0	8.0×10^{-28}‡	5.6×10^{-26}	3.6×10^{-26}	4.1×10^{-7}	3.2×10^{31}	45
J0024−7204S	353.31	706.61	-5.6×10^{-15}	4.0	8.0×10^{-28}‡	6.9×10^{-26}	6.1×10^{-26}	4.6×10^{-7}	3.6×10^{31}	76
J0024−7204T	131.78	263.56	-2.1×10^{-15}	4.0	8.0×10^{-28}‡	3.3×10^{-26}	3.8×10^{-26}	2.0×10^{-6}	1.6×10^{32}	47
J0024−7204U	230.26	460.53	-4.9×10^{-15}	4.0	9.3×10^{-28}†	5.7×10^{-26}	4.1×10^{-26}	7.2×10^{-7}	5.6×10^{31}	43
J0024−7204Y	455.24	910.47	-7.2×10^{-15}	4.0	8.0×10^{-28}‡	9.4×10^{-26}	7.2×10^{-26}	3.3×10^{-7}	2.6×10^{31}	90
J0030+0451	205.53	411.06	-4.3×10^{-16}	0.3	4.1×10^{-27}†	...	7.2×10^{-26}	1.1×10^{-7}	8.7×10^{30}	17
J0034−0534	532.71	1065.43	-1.5×10^{-16}	1.0	4.4×10^{-28}†	...	1.8×10^{-25}	1.5×10^{-7}	1.1×10^{31}	410
J0218+4232	430.46	860.92	-1.4×10^{-14}	5.8	7.9×10^{-28}†	1.5×10^{-25}	8.7×10^{-26}	6.5×10^{-7}	5.0×10^{31}	110
J0307+7443	316.85	633.70	-1.7×10^{-15}	0.6#	3.3×10^{-27}	...	8.6×10^{-26}	1.1×10^{-7}	8.9×10^{30}	26
J0340+41	303.09	606.18	-6.5×10^{-16}	2.7	4.4×10^{-28}	...	5.6×10^{-26}	3.8×10^{-7}	3.0×10^{31}	130
J0407+1607	38.91	77.82	-1.2×10^{-16}	4.1	3.5×10^{-28}	6.2×10^{-26}	5.1×10^{-26}	3.2×10^{-5}	2.5×10^{33}	140
J0437−4715	173.69	347.38	-4.1×10^{-16}	0.2	7.8×10^{-27}†	5.7×10^{-25}	1.2×10^{-25}	1.6×10^{-7}	1.2×10^{31}	16
J0605+3757[d]	366.58	733.15	-6.5×10^{-16}	0.7#	1.6×10^{-27}	...	9.3×10^{-26}	1.1×10^{-7}	8.6×10^{30}	59
J0610−2100	258.98	517.96	-2.3×10^{-16}	5.6	1.3×10^{-28}†	...	7.9×10^{-26}	1.6×10^{-6}	1.2×10^{32}	590
J0613−0200	326.60	653.20	-9.4×10^{-16}	0.9	1.5×10^{-27}†	1.1×10^{-25}	5.6×10^{-26}	1.1×10^{-7}	8.6×10^{30}	37
J0614−3329	317.59	635.19	-1.7×10^{-15}	3.0	6.4×10^{-28}	...	8.5×10^{-26}	5.9×10^{-7}	4.5×10^{31}	130
J0621+1002	34.66	69.31	-5.5×10^{-17}	1.9	5.4×10^{-28}†	1.5×10^{-25}	9.6×10^{-26}	3.6×10^{-5}	2.7×10^{33}	180
J0711−6830	182.12	364.23	-2.9×10^{-16}	1.0	9.8×10^{-28}†	5.0×10^{-26}	3.4×10^{-26}	2.5×10^{-7}	2.0×10^{31}	35
J0737−3039A	44.05	88.11	-3.4×10^{-15}	1.1	6.5×10^{-27}†	7.8×10^{-26}	6.0×10^{-26}	8.0×10^{-6}	6.2×10^{32}	9.2
J0751+1807	287.46	574.92	-6.3×10^{-16}	0.4	3.0×10^{-27}†	1.6×10^{-25}	1.1×10^{-25}	1.2×10^{-7}	9.6×10^{30}	36
J0900−3144	90.01	180.02	-4.0×10^{-16}	0.8	2.1×10^{-27}	...	1.8×10^{-25}	4.3×10^{-6}	3.3×10^{32}	88
J1012+5307	190.27	380.54	-4.1×10^{-16}	0.7	1.7×10^{-27}†	6.9×10^{-26}	4.6×10^{-26}	2.1×10^{-7}	1.6×10^{31}	27
J1017−7156	427.62	855.24	-3.1×10^{-16}	8.1	8.5×10^{-29}	...	1.0×10^{-25}	1.1×10^{-6}	8.3×10^{31}	1200
J1022+1001	60.78	121.56	-1.6×10^{-16}	0.5	2.5×10^{-27}	4.5×10^{-26}	4.8×10^{-26}	1.6×10^{-6}	1.2×10^{32}	19
J1024−0719	193.72	387.43	1.3×10^{-16}	0.5	1.3×10^{-27}†	5.0×10^{-26}	4.6×10^{-26}	1.4×10^{-7}	1.1×10^{31}	35
J1038+0032	34.66	69.32	-7.8×10^{-17}	2.4	5.1×10^{-28}	...	1.2×10^{-25}	5.5×10^{-5}	4.3×10^{33}	230
J1045−4509	133.79	267.59	-3.1×10^{-16}	0.2	5.3×10^{-27}†	4.3×10^{-26}	3.0×10^{-26}	9.3×10^{-8}	7.2×10^{30}	5.7
J1231−1411	271.45	542.91	1.6×10^{-15}	0.5	4.3×10^{-27}†	...	7.5×10^{-26}	1.1×10^{-7}	8.4×10^{30}	17
J1300+1240	160.81	321.62	-7.9×10^{-16}	0.6	3.0×10^{-27}†	...	4.9×10^{-26}	2.7×10^{-7}	2.1×10^{31}	16
J1301+0833	542.38	1084.76	-3.1×10^{-15}	0.9	2.1×10^{-27}	...	1.1×10^{-25}	7.9×10^{-8}	6.1×10^{30}	51
J1435−6100[a]	106.98	213.95	-2.8×10^{-16}	3.3	4.0×10^{-28}	2.7×10^{-25}	...	1.8×10^{-5}	1.4×10^{33}	670
J1453+1902	172.64	345.29	-3.2×10^{-16}	0.9	1.2×10^{-27}†	...	1.4×10^{-25}	1.0×10^{-6}	8.0×10^{31}	120
J1455−3330	125.20	250.40	-2.5×10^{-16}	0.7	1.5×10^{-27}†	5.1×10^{-26}	3.6×10^{-26}	4.1×10^{-7}	3.1×10^{31}	24
J1518+0204A	180.06	360.13	-2.9×10^{-15}	8.0	4.0×10^{-28}‡	...	7.8×10^{-26}	4.6×10^{-6}	3.5×10^{32}	190
J1518+4904	24.43	48.86	-1.3×10^{-17}	0.7	8.5×10^{-28}†	...	2.9×10^{-25}	8.1×10^{-5}	6.2×10^{33}	340
J1537+1155	26.38	52.76	-1.6×10^{-15}	1.0	6.3×10^{-27}†	...	2.4×10^{-25}	8.4×10^{-5}	6.5×10^{33}	39
J1600−3053	277.94	555.88	-6.5×10^{-16}	2.4	5.1×10^{-28}†	5.6×10^{-26}	6.7×10^{-26}	4.9×10^{-7}	3.8×10^{31}	130
J1603−7202	67.38	134.75	-5.4×10^{-17}	1.6	4.4×10^{-28}†	2.3×10^{-26}	2.3×10^{-26}	1.9×10^{-6}	1.5×10^{32}	51
J1614−2230	317.38	634.76	3.9×10^{-16}	1.8	5.0×10^{-28}†	...	6.4×10^{-26}	2.7×10^{-7}	2.1×10^{31}	130
J1623−2631	90.29	180.57	-5.1×10^{-15}	2.2	2.7×10^{-27}†	5.7×10^{-26}	5.1×10^{-26}	3.3×10^{-6}	2.5×10^{32}	19
J1629−6902[a]	166.65	333.30	-2.8×10^{-16}	1.4	7.7×10^{-28}	3.2×10^{-25}	...	3.8×10^{-6}	2.9×10^{32}	420
J1630+3734[d]	301.38	602.75	-8.9×10^{-16}	0.9#	1.5×10^{-27}	...	9.0×10^{-26}	2.2×10^{-7}	1.7×10^{31}	60
J1640+2224	316.12	632.25	-1.6×10^{-16}	1.2	4.9×10^{-28}†	6.7×10^{-26}	5.1×10^{-26}	1.4×10^{-7}	1.1×10^{31}	110
J1641+3627A	96.36	192.72	-1.5×10^{-15}	7.5	4.3×10^{-28}‡	...	5.0×10^{-26}	9.5×10^{-6}	7.3×10^{32}	120
J1643−1224	216.37	432.75	-8.5×10^{-16}	0.4	3.8×10^{-27}†	4.4×10^{-26}	3.6×10^{-26}	7.6×10^{-8}	5.9×10^{30}	9.4
J1701−3006A	190.78	381.57	-3.0×10^{-15}	6.9	4.7×10^{-28}‡	5.8×10^{-26}	3.6×10^{-26}	1.6×10^{-6}	1.3×10^{32}	78
J1701−3006B[b]	278.25	556.50	2.7×10^{-14}	6.9	4.7×10^{-28}‡	7.6×10^{-26}	...	1.6×10^{-6}	1.2×10^{32}	160
J1701−3006C[b]	131.36	262.72	1.1×10^{-15}	6.9	4.7×10^{-28}‡	3.5×10^{-26}	...	3.3×10^{-6}	2.6×10^{32}	76
J1709+2313	215.93	431.85	-6.9×10^{-17}	1.8	2.5×10^{-28}†	...	9.3×10^{-26}	8.6×10^{-7}	6.7×10^{31}	370
J1713+0747	218.81	437.62	-3.9×10^{-16}	1.1	1.0×10^{-27}†	4.5×10^{-26}	3.5×10^{-26}	1.8×10^{-7}	1.4×10^{31}	34
J1719−1438	172.71	345.41	-2.3×10^{-16}	1.6	5.8×10^{-28}	...	1.6×10^{-25}	2.0×10^{-6}	1.6×10^{32}	270
J1721−2457	285.99	571.98	-2.4×10^{-16}	1.6	4.7×10^{-28}†	...	5.5×10^{-26}	2.5×10^{-7}	1.9×10^{31}	120

TABLE 8 — *Continued*

Pulsar	$f_{\rm rot}$ (Hz)	$f_{\rm gw}$ (Hz)	$\dot{f}_{\rm rot}$ (Hz/s)	d (kpc)	$h_0^{\rm sd}$	prior $h_0^{95\%}$	S6/VSR2,4 $h_0^{95\%}$	ε	Q_{22} (kg m^2)	$h_0^{95\%}/h_0^{\rm sd}$
J1730−2304	123.11	246.22	-3.1×10^{-16}	0.5	2.5×10^{-27}	5.8×10^{-26}	4.5×10^{-26}	3.6×10^{-7}	2.8×10^{31}	18
J1731−1847	426.52	853.04	-4.6×10^{-15}	4.0	6.6×10^{-28}	···	1.3×10^{-25}	6.6×10^{-7}	5.1×10^{31}	190
J1732−5049	188.23	376.47	-5.0×10^{-16}	1.8	7.3×10^{-28}	5.3×10^{-26}	4.6×10^{-26}	5.6×10^{-7}	4.3×10^{31}	63
J1738+0333	170.94	341.87	-6.7×10^{-16}	2.0	8.1×10^{-28}†	···	1.1×10^{-25}	1.8×10^{-6}	1.4×10^{32}	140
J1741+1351	266.87	533.74	-2.2×10^{-15}	1.4	1.6×10^{-27}	···	1.1×10^{-25}	5.1×10^{-7}	3.9×10^{31}	67
J1744−1134	245.43	490.85	-4.3×10^{-16}	0.4	2.5×10^{-27}†	1.1×10^{-25}	6.3×10^{-26}	1.0×10^{-7}	8.0×10^{30}	25
J1745−0952	51.61	103.22	-7.6×10^{-17}	2.4	4.1×10^{-28}†	···	6.0×10^{-26}	1.3×10^{-5}	9.8×10^{32}	150
J1748−2446A	86.48	172.96	-1.4×10^{-15}	5.5	5.8×10^{-28}‡	3.9×10^{-26}	3.2×10^{-26}	5.6×10^{-6}	4.3×10^{32}	55
J1748−2446C	118.54	237.08	-1.9×10^{-15}	5.5	5.8×10^{-28}‡	5.0×10^{-26}	3.8×10^{-26}	3.5×10^{-6}	2.7×10^{32}	65
J1748−2446D	212.14	424.27	-3.4×10^{-15}	5.5	5.8×10^{-28}‡	6.8×10^{-26}	5.3×10^{-26}	1.5×10^{-6}	1.2×10^{32}	91
J1748−2446E	455.00	910.00	-7.2×10^{-15}	5.5	5.8×10^{-28}‡	9.0×10^{-26}	7.3×10^{-26}	4.6×10^{-7}	3.6×10^{31}	130
J1748−2446F	180.50	361.00	-2.9×10^{-15}	5.5	5.8×10^{-28}‡	8.3×10^{-26}	7.4×10^{-26}	3.0×10^{-6}	2.3×10^{32}	130
J1748−2446G	46.14	92.29	-7.3×10^{-16}	5.5	5.8×10^{-28}‡	5.9×10^{-26}	4.5×10^{-26}	2.8×10^{-5}	2.1×10^{33}	78
J1748−2446H	203.01	406.02	-3.2×10^{-15}	5.5	5.8×10^{-28}‡	7.8×10^{-26}	5.8×10^{-26}	1.8×10^{-6}	1.4×10^{32}	99
J1748−2446I	104.49	208.98	-1.7×10^{-15}	5.5	5.8×10^{-28}‡	3.6×10^{-26}	3.7×10^{-26}	4.5×10^{-6}	3.4×10^{32}	64
J1748−2446K	336.74	673.48	-5.3×10^{-15}	5.5	5.8×10^{-28}‡	6.8×10^{-26}	5.9×10^{-26}	6.8×10^{-7}	5.3×10^{31}	100
J1748−2446L	445.49	890.99	-7.1×10^{-15}	5.5	5.8×10^{-28}‡	1.4×10^{-25}	1.1×10^{-25}	7.5×10^{-7}	5.8×10^{31}	200
J1748−2446M	280.15	560.29	-4.4×10^{-15}	5.5	5.8×10^{-28}‡	1.0×10^{-25}	9.5×10^{-26}	1.6×10^{-6}	1.2×10^{32}	160
J1748−2446N	115.38	230.76	-1.8×10^{-15}	5.5	5.8×10^{-28}‡	5.8×10^{-26}	6.4×10^{-26}	6.3×10^{-6}	4.8×10^{32}	110
J1748−2446O	596.44	1192.87	-9.4×10^{-15}	5.5	5.8×10^{-28}‡	2.6×10^{-25}	2.6×10^{-25}	9.6×10^{-7}	7.4×10^{31}	450
J1748−2446P[b]	578.50	1157.00	-8.7×10^{-14}	5.5	5.8×10^{-28}‡	1.6×10^{-25}	···	6.1×10^{-7}	4.8×10^{31}	267
J1748−2446Q	355.64	711.29	-5.6×10^{-15}	5.5	5.8×10^{-28}‡	8.8×10^{-26}	9.4×10^{-26}	9.7×10^{-7}	7.5×10^{31}	160
J1748−2446R	198.86	397.73	-3.2×10^{-15}	5.5	5.8×10^{-28}‡	8.1×10^{-26}	5.1×10^{-26}	1.7×10^{-6}	1.3×10^{32}	87
J1748−2446S	163.49	326.98	-2.6×10^{-15}	5.5	5.8×10^{-28}‡	4.5×10^{-26}	5.3×10^{-26}	2.6×10^{-6}	2.0×10^{32}	91
J1748−2446T	141.15	282.29	-2.2×10^{-15}	5.5	5.8×10^{-28}‡	5.1×10^{-26}	3.0×10^{-26}	2.0×10^{-6}	1.5×10^{32}	52
J1748−2446U	304.03	608.06	-4.8×10^{-15}	5.5	5.8×10^{-28}‡	···	1.4×10^{-25}	1.9×10^{-6}	1.5×10^{32}	230
J1748−2446V	482.51	965.02	-7.6×10^{-15}	5.5	5.8×10^{-28}‡	1.3×10^{-25}	1.3×10^{-25}	7.2×10^{-7}	5.6×10^{31}	220
J1748−2446W	237.80	475.60	-3.8×10^{-15}	5.5	5.8×10^{-28}‡	9.4×10^{-26}	9.5×10^{-26}	2.2×10^{-6}	1.7×10^{32}	160
J1748−2446X	333.42	666.83	-5.3×10^{-15}	5.5	5.8×10^{-28}‡	8.3×10^{-26}	4.8×10^{-26}	5.7×10^{-7}	4.4×10^{31}	83
J1748−2446Y	488.24	976.49	-7.7×10^{-15}	5.5	5.8×10^{-28}‡	2.1×10^{-25}	2.1×10^{-25}	1.2×10^{-6}	9.0×10^{31}	370
J1748−2446Z	406.08	812.15	-6.4×10^{-15}	5.5	5.8×10^{-28}‡	8.5×10^{-26}	8.6×10^{-26}	6.8×10^{-7}	5.2×10^{31}	150
J1748−2446aa	172.77	345.54	-2.7×10^{-15}	5.5	5.8×10^{-28}‡	2.3×10^{-25}	1.5×10^{-25}	6.6×10^{-6}	5.1×10^{32}	260
J1748−2446ab	195.32	390.65	-3.1×10^{-15}	5.5	5.8×10^{-28}‡	4.7×10^{-26}	4.0×10^{-26}	1.4×10^{-6}	1.1×10^{32}	69
J1748−2446ac	196.58	393.17	-3.1×10^{-15}	5.5	5.8×10^{-28}‡	7.2×10^{-26}	5.6×10^{-26}	1.9×10^{-6}	1.5×10^{32}	97
J1748−2446ad[b]	716.36	1432.70	1.7×10^{-14}	5.5	5.8×10^{-28}‡	1.8×10^{-25}	···	4.5×10^{-7}	3.5×10^{31}	300
J1748−2446ae	273.33	546.66	-4.3×10^{-15}	5.5	5.8×10^{-28}‡	6.6×10^{-26}	6.8×10^{-26}	1.2×10^{-6}	9.2×10^{31}	120
J1748−2446af	302.63	605.26	-4.8×10^{-15}	5.5	5.8×10^{-28}‡	1.1×10^{-25}	6.0×10^{-26}	8.5×10^{-7}	6.5×10^{31}	100
J1748−2446ag	224.82	449.64	-3.6×10^{-15}	5.5	5.8×10^{-28}‡	9.4×10^{-26}	5.1×10^{-26}	1.3×10^{-6}	1.0×10^{32}	87
J1748−2446ah	201.40	402.81	-3.2×10^{-15}	5.5	5.8×10^{-28}‡	5.5×10^{-26}	4.0×10^{-26}	1.3×10^{-6}	10.0×10^{31}	69
J1748−2446ai	47.11	94.21	-7.5×10^{-16}	5.5	5.8×10^{-28}‡	···	1.6×10^{-25}	9.2×10^{-5}	7.1×10^{33}	270
J1751−2857	255.44	510.87	-7.3×10^{-16}	1.4	9.5×10^{-28}	···	6.8×10^{-26}	3.6×10^{-7}	2.8×10^{31}	72
J1756−2251	35.14	70.27	-1.3×10^{-15}	2.9	1.7×10^{-27}	9.7×10^{-26}	7.4×10^{-26}	4.1×10^{-5}	3.2×10^{33}	45
J1757−5322[a]	112.74	225.48	-3.3×10^{-16}	1.4	1.0×10^{-27}	3.7×10^{-25}	···	9.4×10^{-6}	7.3×10^{32}	360
J1801−1417	275.85	551.71	3.1×10^{-16}	1.8	4.8×10^{-28}†	6.2×10^{-26}	7.3×10^{-26}	4.1×10^{-7}	3.1×10^{31}	150
J1801−3210	134.16	268.33	1.8×10^{-17}	5.0	5.8×10^{-29}	···	3.5×10^{-26}	2.3×10^{-6}	1.8×10^{32}	610
J1802−2124	79.07	158.13	-4.4×10^{-16}	3.3	5.7×10^{-28}†	···	4.7×10^{-26}	6.0×10^{-6}	4.6×10^{32}	83
J1803−30	140.82	281.63	-2.2×10^{-15}	7.8	4.1×10^{-28}‡	5.5×10^{-26}	4.1×10^{-26}	3.8×10^{-6}	3.0×10^{32}	100
J1804−0735	43.29	86.58	-6.9×10^{-16}	8.4	3.8×10^{-28}‡	8.4×10^{-26}	8.8×10^{-26}	9.4×10^{-5}	7.2×10^{33}	230
J1804−2717	107.03	214.06	-4.7×10^{-16}	1.2	1.4×10^{-27}	2.4×10^{-26}	2.2×10^{-26}	5.3×10^{-7}	4.1×10^{31}	15
J1807−2459A	326.86	653.71	-5.2×10^{-15}	2.7	1.2×10^{-27}‡	1.5×10^{-25}	9.6×10^{-26}	5.8×10^{-7}	4.5×10^{31}	81
J1810+1744	601.41	1202.82	-1.6×10^{-15}	2.5	5.3×10^{-28}	···	1.8×10^{-25}	2.9×10^{-7}	2.3×10^{31}	340
J1810−2005	30.47	60.93	-5.0×10^{-17}	4.0	2.6×10^{-28}†	2.2×10^{-25}	1.6×10^{-25}	1.6×10^{-4}	1.3×10^{34}	630
J1811−2405	375.86	751.71	-1.9×10^{-15}	1.7	1.1×10^{-27}	···	8.5×10^{-26}	2.4×10^{-7}	1.9×10^{31}	80
J1823−3021A	183.82	367.65	-2.9×10^{-15}	7.9	4.1×10^{-28}‡	4.0×10^{-26}	3.5×10^{-26}	1.9×10^{-6}	1.5×10^{32}	86
J1824−2452A	327.41	654.81	-1.7×10^{-13}	5.5	3.4×10^{-27}†	7.9×10^{-26}	5.5×10^{-26}	6.7×10^{-7}	5.2×10^{31}	16
J1824−2452B[b]	152.75	305.50	5.6×10^{-15}	5.5	5.8×10^{-28}‡	4.2×10^{-26}	···	2.3×10^{-6}	1.8×10^{32}	72
J1824−2452C[b]	240.48	480.96	-9.8×10^{-15}	5.5	5.8×10^{-28}‡	6.6×10^{-26}	···	1.5×10^{-6}	1.2×10^{32}	110
J1824−2452E[b]	184.53	369.06	3.7×10^{-15}	5.5	5.8×10^{-28}‡	7.5×10^{-26}	···	2.9×10^{-6}	2.2×10^{32}	130
J1824−2452F[b]	407.97	815.94	-1.6×10^{-15}	5.5	5.8×10^{-28}‡	9.8×10^{-26}	···	7.6×10^{-7}	5.9×10^{31}	170
J1824−2452G[b]	169.23	338.46	-5.2×10^{-15}	5.5	5.8×10^{-28}‡	7.3×10^{-26}	···	3.3×10^{-6}	2.6×10^{32}	130
J1824−2452H[b]	216.01	432.02	-3.6×10^{-15}	5.5	5.8×10^{-28}‡	8.2×10^{-26}	···	2.3×10^{-6}	1.8×10^{32}	140
J1824−2452I[c]	254.33	508.67	-5.4×10^{-15}	5.5	5.8×10^{-28}‡	2.2×10^{-25}	···	4.4×10^{-6}	3.4×10^{32}	370
J1824−2452J[b]	247.54	495.08	4.7×10^{-15}	5.5	5.8×10^{-28}‡	1.1×10^{-25}	···	2.3×10^{-6}	1.7×10^{32}	180
J1841+0130	33.59	67.18	-9.2×10^{-15}	3.2	4.2×10^{-27}	1.6×10^{-25}	1.3×10^{-25}	8.7×10^{-5}	6.7×10^{33}	31
J1843−1113	541.81	1083.62	-2.8×10^{-15}	2.0	9.3×10^{-28}	1.6×10^{-25}	1.1×10^{-25}	1.8×10^{-7}	1.4×10^{31}	120
J1853+1303	244.39	488.78	-5.1×10^{-16}	1.6	7.3×10^{-28}†	···	8.5×10^{-26}	5.4×10^{-7}	4.2×10^{31}	120
J1857+0943	186.49	372.99	-6.1×10^{-16}	0.9	1.6×10^{-27}†	7.3×10^{-26}	5.7×10^{-26}	3.5×10^{-7}	2.7×10^{31}	35
J1903+0327	465.14	930.27	-3.8×10^{-15}	6.5	3.6×10^{-28}†	···	1.6×10^{-25}	1.1×10^{-6}	8.8×10^{31}	450

TABLE 8 — *Continued*

Pulsar	$f_{\rm rot}$ (Hz)	$f_{\rm gw}$ (Hz)	$\dot{f}_{\rm rot}$ (Hz/s)	d (kpc)	$h_0^{\rm sd}$	prior $h_0^{95\%}$	S6/VSR2,4 $h_0^{95\%}$	ε	Q_{22} (kg m^2)	$h_0^{95\%}/h_0^{\rm sd}$
J1905+0400	264.24	528.48	-2.8×10^{-16}	1.3	6.3×10^{-28}†	7.4×10^{-26}	5.0×10^{-26}	2.3×10^{-7}	1.8×10^{31}	80
J1909−3744	339.32	678.63	-1.9×10^{-16}	1.3	4.7×10^{-28}†	8.2×10^{-26}	5.9×10^{-26}	1.5×10^{-7}	1.2×10^{31}	120
J1910+1256	200.66	401.32	-3.4×10^{-16}	1.9	5.4×10^{-28}†	···	7.7×10^{-26}	8.8×10^{-7}	6.8×10^{31}	140
J1910−5959A	306.17	612.33	-1.9×10^{-16}	4.5	1.4×10^{-28}†	7.7×10^{-26}	5.5×10^{-26}	6.2×10^{-7}	4.8×10^{31}	390
J1910−5959B	119.65	239.30	-1.9×10^{-15}	4.5	7.1×10^{-28}‡	3.8×10^{-26}	2.5×10^{-26}	1.9×10^{-6}	1.4×10^{32}	35
J1910−5959C	189.49	378.98	1.1×10^{-18}	4.5	1.4×10^{-29}†	4.4×10^{-26}	3.2×10^{-26}	9.5×10^{-7}	7.4×10^{31}	2300
J1910−5959D	110.68	221.35	-1.8×10^{-15}	4.5	7.1×10^{-28}‡	3.1×10^{-26}	2.1×10^{-26}	1.8×10^{-6}	1.4×10^{32}	29
J1910−5959E	218.73	437.47	-3.5×10^{-15}	4.5	7.1×10^{-28}‡	4.8×10^{-26}	3.6×10^{-26}	8.0×10^{-7}	6.1×10^{31}	50
J1911+0101A[a]	276.36	552.71	5.0×10^{-16}	7.4	4.3×10^{-28}‡	6.0×10^{-25}	···	1.4×10^{-5}	1.1×10^{33}	1400
J1911+0101B[a]	185.72	371.45	6.9×10^{-17}	7.4	4.3×10^{-28}‡	7.4×10^{-25}	···	3.8×10^{-5}	2.9×10^{33}	1700
J1911+1347	216.17	432.34	-7.9×10^{-16}	1.6	9.6×10^{-28}	7.0×10^{-26}	4.8×10^{-26}	3.9×10^{-7}	3.0×10^{31}	50
J1911−1114	275.81	551.61	-4.7×10^{-16}	1.6	6.7×10^{-28}†	5.7×10^{-26}	6.3×10^{-26}	3.1×10^{-7}	2.4×10^{31}	94
J1918−0642	130.79	261.58	-4.0×10^{-16}	1.4	1.0×10^{-27}†	···	4.0×10^{-26}	7.7×10^{-7}	6.0×10^{31}	39
J1939+2134	641.93	1283.86	-4.3×10^{-14}	5.0	1.3×10^{-27}†	1.8×10^{-25}	1.3×10^{-25}	3.6×10^{-7}	2.8×10^{31}	96
J1944+0907	192.86	385.71	-3.6×10^{-16}	1.3	8.6×10^{-28}†	···	5.5×10^{-26}	4.4×10^{-7}	3.4×10^{31}	64
J1955+2908	163.05	326.10	-7.5×10^{-16}	5.4	3.2×10^{-28}†	7.0×10^{-26}	5.4×10^{-26}	2.6×10^{-6}	2.0×10^{32}	170
J1959+2048	622.12	1244.24	-4.4×10^{-15}	1.5	1.4×10^{-27}†	···	1.5×10^{-25}	1.4×10^{-7}	1.1×10^{31}	110
J2007+2722	40.82	81.64	-1.6×10^{-15}	6.8	7.4×10^{-28}	···	7.1×10^{-26}	6.9×10^{-5}	5.3×10^{33}	96
J2010−1323	191.45	382.90	-1.8×10^{-16}	1.3	6.0×10^{-28}	···	6.3×10^{-26}	5.2×10^{-7}	4.0×10^{31}	100
J2017+0603	345.28	690.56	-9.6×10^{-16}	1.3	1.0×10^{-27}	···	1.3×10^{-25}	3.4×10^{-7}	2.6×10^{31}	130
J2019+2425	254.16	508.32	-1.7×10^{-16}	0.9	7.2×10^{-28}†	9.2×10^{-26}	5.6×10^{-26}	1.9×10^{-7}	1.4×10^{31}	79
J2033+17	168.10	336.19	-2.3×10^{-16}	1.4	6.8×10^{-28}†	7.5×10^{-26}	8.0×10^{-26}	9.2×10^{-7}	7.1×10^{31}	120
J2043+1711	420.19	840.38	-7.3×10^{-16}	1.1	9.4×10^{-28}†	···	7.3×10^{-26}	1.1×10^{-7}	8.5×10^{30}	78
J2051−0827	221.80	443.59	-6.1×10^{-16}	1.3	1.0×10^{-27}†	7.5×10^{-26}	5.3×10^{-26}	3.3×10^{-7}	2.5×10^{31}	51
J2124−3358	202.79	405.59	-4.4×10^{-16}	0.3	4.0×10^{-27}†	4.9×10^{-26}	3.9×10^{-26}	6.7×10^{-8}	5.2×10^{30}	9.9
J2129−5721	268.36	536.72	-1.5×10^{-15}	0.4	4.7×10^{-27}†	6.2×10^{-26}	5.2×10^{-26}	6.8×10^{-8}	5.3×10^{30}	11
J2140−2310A	90.75	181.50	-1.4×10^{-15}	9.2	3.5×10^{-28}‡	···	5.9×10^{-26}	1.6×10^{-5}	1.2×10^{33}	170
J2145−0750	62.30	124.59	-1.0×10^{-16}	0.6	1.8×10^{-27}†	3.8×10^{-26}	2.9×10^{-26}	1.0×10^{-6}	7.9×10^{31}	16
J2214+3000	320.59	641.18	-1.5×10^{-15}	1.3	1.3×10^{-27}	···	7.2×10^{-26}	2.2×10^{-7}	1.7×10^{31}	54
J2215+5135	383.20	766.40	-4.1×10^{-15}	3.3	8.0×10^{-28}	···	1.6×10^{-25}	8.7×10^{-7}	6.7×10^{31}	200
J2229+2643	335.82	671.63	1.7×10^{-16}	1.4	4.1×10^{-28}†	9.9×10^{-26}	6.5×10^{-26}	2.0×10^{-7}	1.5×10^{31}	160
J2241−5236	457.31	914.62	-1.4×10^{-15}	0.7	2.1×10^{-27}	···	8.9×10^{-26}	6.9×10^{-8}	5.3×10^{30}	42
J2302+4442	192.59	385.18	-5.1×10^{-16}	0.8	1.8×10^{-27}	···	4.5×10^{-26}	2.2×10^{-7}	1.7×10^{31}	26
J2317+1439	290.25	580.51	-1.3×10^{-16}	1.9	2.8×10^{-28}†	8.8×10^{-26}	5.6×10^{-26}	3.0×10^{-7}	2.3×10^{31}	200
J2322+2057	207.97	415.94	-1.8×10^{-16}	0.8	9.6×10^{-28}†	1.1×10^{-25}	5.4×10^{-26}	2.3×10^{-7}	1.8×10^{31}	57

NOTE. — Detector calibration errors mean that for pulsars with $f_{\rm gw}$ below and above 50 Hz there are ∼6% and ∼20% uncertainties on these limits respectively.

† The pulsar's spin-down is corrected for proper motion effects.

‡ The pulsar's spin-down is calculated using a characteristic spin-down age of 10^9 years.

The pulsar's distance is calculated using the NE2001 model of Cordes & Lazio (2002).

[a] Results from S3/S4 (Abbott et al. 2007b)

[b] Results from S5 (Abbott et al. 2010).

[c] New result from S5 using data covering 2006.

[d] Recently discovered pulsar with timing solution from after the end of S6 or VSR4. As this is an MSP the timing solution should extrapolate back well over the search period and it is unlikely that any glitches occurred.